JAERI-Research
2004-015

JP0450790

INTEGRAL EXPERIMENTS FOR VERIFICATION OF TRITIUM PRODUCTION ON THE BERYLLIUM/LITHIUM TITANATE BLANKET MOCK-UP WITH A ONE-BREEDER LAYER

October 2004

Yury M.VERZILOV, Satoshi SATO, Makoto NAKAO
Kentaro OCHIAI, Masayuki WADA* and Takeo NISHITANI

日本原子力研究所
Japan Atomic Energy Research Institute

本レポートは，日本原子力研究所が不定期に公刊している研究報告書です。
入手の問合わせは，日本原子力研究所研究情報部研究情報課（〒319-1195 茨城県那珂郡東海村）あて，お申し越しください。なお，このほかに財団法人原子力弘済会資料センター（〒319-1195 茨城県那珂郡東海村日本原子力研究所内）で複写による実費頒布をおこなっております。

This report is issued irregularly.
Inquiries about availability of the reports should be addressed to Research Information Division, Department of Intellectual Resources, Japan Atomic Energy Research Institute, Tokai-mura, Naka-gun, Ibarakiken 319-1195, Japan.

© Japan Atomic Energy Research Institute, 2004
編集兼発行　日本原子力研究所

Integral Experiments for Verification of Tritium Production on the Beryllium/Lithium Titanate Blanket Mock-up with a One-breeder Layer

Yury M.VERZILOV※, Satoshi SATO, Makoto NAKAO, Kentaro OCHIAI,
Masayuki WADA* and Takeo NISHITANI

Department of Fusion Engineering Research
(Tokai Site)
Naka Fusion Research Establishment
Japan Atomic Energy Research Institute
Tokai-mura, Naka-gun, Ibaraki-ken

(Received August 26, 2004)

The first series of integral experiments on the blanket mock-up with a one breeder layer was performed in support of the concept of the solid breeding blanket cooled with water, proposed by JAERI for application in the DEMO reactor. The mock-up for the first series of experiments was designed to be as simple as possible within the proposed blanket concept. Key objectives of the experiments were: to check how correctly the tritium production rate can be predicted in the breeder layer closest to the first wall, since this particular location is greatly affected by changes of incoming neutron spectra; to validate the modified experimental techniques for measurements of tritium production rate in conditions of quick gradient thermal neutron field inside the lithium titanate layer. The mock-up contains F82H, lithium titanate and beryllium layers, with respective thicknesses of 16 mm, 12 mm and 203 mm. An additional tungsten layer was installed in front of the first layer in order to simulate armor material. The mock-up, being placed inside the SS316 cylindrical enclosure, is shaped as a pseudo-cylindrical slab with an area-equivalent diameter of 628 mm. Integral experiments on the blanket mock-up irradiated by neutrons from the D-T source with and without the source reflector were executed. A detailed description of experimental results and an example of calculation analysis are presented.

Keywords: D-T Neutron Source, Source Reflector, Fusion Reactor, Blanket, Beryllium, Lithium Titanate, Tritium Production Rate, Integral Experiment, FNS

※ JAERI Research Fellow

* Startcom Co., Ltd.

ベリリウム／チタン酸リチウムブランケット単一増殖層模擬体系における トリチウム生成確証のための積分実験

日本原子力研究所那珂研究所核融合工学部
Yury M.VERZILOV※・佐藤　聡・中尾　誠・落合　謙太郎・和田　政行*・西谷　健夫

(2004年8月26日受理)

原研が提案しているDEMO炉の水冷却固体増殖ブランケット概念に対する単一増殖層模擬体系を用いて第1回の一連の積分実験を実施した。第1回の一連の実験の模擬体系は提案している概念の範囲で、できるかぎり単純になるよう計画した。実験の主要目的は　入射中性子のスペクトルに影響され易い第1壁近傍の増殖層のトリチウム生成率をどれだけ正確に予測できるかを確認することと、チタン酸リチウム層内で急激に変化する熱中性子場において改善した実験手法を確認することである。模擬体系は、16mm厚のF82H、12mm厚のチタン酸リチウム及び203mm厚のベリリウム層から成っている。またアーマー材を模擬するためにタングステン層を第1層の前面に追加した。模擬体系は面積等価直径628mmの疑似円筒形状のSS316容器内に設置した。模擬体系に対する積分実験は中性子源反射体付きと無しのD-T中性子源で照射して実施した。本報告では実験結果の解析計算の詳細について述べる。

那珂研究所（東海駐在）：〒319-1195 茨城県那珂郡東海村白方白根2-4
※　原研リサーチフェロー
*　スタートコム（株）

Contents

目　次

1. Introduction

Due to the necessity of tritium breeding for self-sufficiency of the D-T fusion reactor, the blanket is considered the most significant nuclear component of the reactor. In order to meet self-sufficiency requirements, a comprehensive verification of neutronics design calculations has to be done throughout experiments on the design-oriented blanket mock-ups. Previous blanket experiments related to tritium breeding issues were performed for conceptual design purposes of the fusion [1], and hybrid (fission-fusion) [2] reactors, and thus do not reflect the present status of design work on the DEMO reactor. Some concepts of the solid breeding blanket cooled with water have been proposed for application in the DEMO reactor by JAERI [3,4]. Integral experiments for verification of tritium breeding must meet certain criteria, specified by the blanket design, for example, the tritium breeding ratio design margin, and closely simulate all reactor design aspects relevant to neutronics. Therefore, experiments must be performed in conditions that closely simulate:

- ✓ a blanket module;
- ✓ a fusion reactor environment.

A mock-up with a multi-layer configuration containing a variety of materials utilized for structural, tritium breeding, neutron multiplier and coolant functions, is able to correctly simulate the blanket module. In addition, in order to verify the impact of plasma facing component on nuclear performance [5], appropriate material must be added to the mock-up configuration.

Primarily, due to the absence of the volumetric neutron source, a more complicated situation exists for simulation of the fusion reactor environment. At this time, experiments can be executed exclusively with the use of the point D-T neutron source with two variant arrangements: with or without the source reflector. In the first case neutrons entering the mock-up contain only high energy neutrons from the source. In the second case neutrons entering the mock-up contain high energy neutrons from the source and low energy neutrons reflected from materials located around the source. The described experimental arrangement allows certain simulation of the neutron environment for the blanket mock-up.

The first series of reported integral experiments on a one breeder layer mock-up were performed in the verification activity frame for the developed blanket concept [4]. Future experiments on the mock-ups towards full simulation of the blanket module are scheduled.

The mock-up for the first series of experiments was designed in order to be as simple as possible within the proposed blanket concept. The key experiment objectives were:

- ✓ to check how correctly the tritium production rate can be predicted in the breeder layer that is closer to the first wall, since this particular location is greatly affected by changes of neutron spectra and introduction of the armor material;
- ✓ to validate the modified experimental techniques for measurement of the tritium production rate in conditions of quick gradient of the thermal neutron field inside the lithium titanate layer.

Regarding these objectives, several experiments on a one breeder layer mock-up were completed.

2. General Description of the DEMO Blanket Module

The blanket design for the DEMO fusion reactor [3] was developed in JAERI [4] (Fig. 1). The blanket has a modular structure consisting of the first wall, solid breeder pebble layers, neutron multiplier pebble layers, and cooling panels with a ferritic steel (F82H) blanket structure. The Li_2TiO_3 and Be pebbles are proposed as candidate materials for the breeder and the multiplier, respectively. The breeder and neutron multiplier pebble beds are separated with a cooling panel to keep their temperature limits. Breeder layers are purged with helium gas in order to collect tritium. The module is cooled with supercritical pressure water.

Performed analysis shows [6] that the required net TBR of approximately 1.05 can be achieved for the proposed blanket design with a lithium-6 enriched breeder bed and the volumetric beryllium to lithium materials ratio of more than four. In such conditions, the beryllium bed produces a significant number of thermalized neutrons, and tritium production mostly occurs through absorption of thermal neutrons by lithium-6, according to the $^6Li(n,\alpha)^3H$ reaction. Due to the large cross section of the reaction and the heterogeneous blanket structure, quick tritium production gradients occur around the lithium and beryllium material boundaries. Tritium production rate distributions are highly typical for the solid type breeder blanket, and thus, special attention must be paid to measuring the detailed tritium production rate distributions inside the breeder layer. In addition, the $^6Li(n,\alpha)^3H$ reaction produces local peaks of nuclear heat around material boundaries. Therefore, results of the

experimental study of tritium production rates, obtained throughout integral experiments, will also be significant from the thermo-mechanical blanket design point of view.

3. Integral Experiment Strategy for Verification of Tritium Production

At the present time absence of the volumetric D-T neutron source is the most significant problem for comprehensive verification of tritium production through integral experiments on the blanket module. Most likely, simulation of the neutron source will be impossible without construction of the ITER reactor. Meanwhile, constructive experiments can be done on the blanket mock-ups irradiated by D-T neutrons from the point neutron source with (or without) the source reflector. The source reflector drastically increases the number of low energy neutrons that enter the tested mock-up and allows some simulation of low energy neutrons reflected at the opposite side of the reactor vacuum chamber. From this point of view, the source reflector must be properly configured in order to simulate the reflected neutron spectrum.

Lastly, it seems as a reasonable solution at this time to perform a series of integral experiments on blanket mock-ups irradiated by neutrons from the point D-T source. Several series of integral experiments on the blanket mock-ups verifying tritium breeding were scheduled for execution at the FNS laboratory. The research principle is based on a step-by-step complication of the blanket mock-up and neutron environment. The complication of the mock-up will be performed by an increase in the number of breeding layers and introduction of additional layers of appropriate materials to simulate:

- ✓ first wall with coolant channels;
- ✓ coolant channels for breeding layers;
- ✓ tungsten armor.

The neutron environment will be simulated by placement of the source reflector.

In the present report, the primary series of experiments on the mock-up with a one breeder layer are presented. The following experiments were performed:

- ✓ irradiation of the mock-up by neutrons from the D-T source;
- ✓ irradiation of the mock-up by neutrons from the D-T source with a reflector;

- ✓ placement of the tungsten armor layer in front of the mock-up and irradiation by neutrons from the D-T source with a reflector.

So far, in order to compare experimental data of the mentioned experiments directly, their performance and arrangement was set up in a similar manner. For that purpose, the first experiment, a mock-up irradiated by neutrons from the D-T source, was considered as the reference case. By analyzing performed experiments, it is possible to study the impact of the following on the tritium production rate (TPR):

- ✓ tungsten armor;
- ✓ incident neutron spectrum;
- ✓ heterogeneous effect.

4. Blanket Mock-up with a One Breeder Layer

4.1. Basic Arrangement

The composition of the blanket mock-up, selected for the primary series of integral experiments, contains several layers of F82H, lithium titanate and beryllium, with respective thicknesses of 16 mm, 12 mm and 203.2 mm. The selected thicknesses of ferritic steel and lithium titanate were a subject to material availability. Beryllium layer thickness was selected as to enhance the tritium production rate on the beryllium and lithium titanate layer boundary. Figure 2 shows result analysis for beryllium layer with thicknesses of 101.6 and 203.2 mm. Based on this comparison, the beryllium layer thickness was selected at 203.2 mm. Figures 3 and 4 show a basic arrangement of the blanket mock-up. The mock-up is shaped as a pseudo-cylindrical slab with an area-equivalent diameter of 628 mm and a total thickness of 231.2 mm. The mock-up placed inside the SS316 cylindrical enclosure is located on a movable platform.

Integral measurements, e.g., reaction rates of activation and tritium production, were carried out by appropriate foils and pellets introduced inside the mock-up during the assembling procedure. Two kinds of measurements were performed in the experiment in order to verify:

- ✓ neutron transport calculation, using foils and pellet detectors distributed through the mock-up;
- ✓ tritium production rates, using diagnostic pellets introduced inside the lithium titanate layer.

Arrangement of foils and pellets for measurement of reaction rates is shown in fig. 5. Detectors were attached to the surface of beryllium blocks as shown in Fig. 6. Figure 7 shows a stack of diagnostic pellets for measurement of the TPR distribution inside the breeder layer. A detailed description of foils and pellets with appropriate measurement techniques is given in Chapter 5.

4.2. Material Specifications and Unit Description

Chemical composition of materials used for construction of breeder and multiplier layers of the blanket mock-up is very important, especially for the present type of the mock-up, mainly due to tritium breeding on lithium-6 by thermal neutrons. Thus, additional analyses were done for beryllium and lithium titanate materials.

4.2.1. Lithium Titanate

Lithium titanate plates were manufactured by Kawasaki Heavy Industries Ltd. (Japan). The plates were produced through cold pressing of lithium titanate powder and a consequent sintering process. All the manufactured plates have dimensions of 50 x 50 x 12 mm. Several blocks have a central hole with a diameter of 13.2 mm for diagnostic pellets. Manufacturer information concerning the powder chemical composition, prior to the sintering procedure, is shown in Table 1. Lithium-6 enrichment in lithium titanate powder equals to 40.33 %.

Table 1 Chemical composition of lithium titanate powder used for plate manufacturing.

Element	Content, w%	Element	Content, w%
Li	10.8	Fe	0.01
Ti	43.6	S	0.03
O	45.5	K	0.06
B	< 0.01	Ca	0.02
C	0.13	Cr	< 0.01
Na	0.01	Ni	< 0.01
Mg	0.01	Cu	< 0.01
Al	0.01	Zr	0.01
Si	0.06		

It is important to note that, according to the lithium titanate chemical formula, Li_2TiO_3, theoretical weight percent of lithium should be equal to 12.2 %. By comparing this value with the value from table 1, 10.8 %, it is possible to conclude that the stoichiometrical ratio of used lithium titanate is different from the theoretical value. In addition, lithium content in the plate can be changed, in comparison with the powder form, due to the sintering process's high temperature. From this point of view, additional analysis was performed in JAERI by the ICP-MS method [7] for the lithium titanate plate. Obtained results are presented in Table 2. Lithium-6 enrichment in the lithium titanate plate equals to 41.37 %.

Table 2 Lithium titanate plate chemical composition.

Element	Content, w%
Li	9.40
O	45.5
Ti	43.6

The listed lithium content data is lower then the powder form data, thus additional analysis is necessary to study uniformity of lithium content inside the plate. Meanwhile, obtained lithium content data should be considered for final analysis of integral experiments.

4.2.2. Beryllium

Standard grade beryllium blocks (S-200-F, Brush Wellman Inc.) were used for construction of the mock-up. The blocks were produced through consolidating beryllium powder by vacuum hot pressing, and afterwards machining the blocks to dimensions listed in Table. 3.

Table 3 Beryllium blocks used for integral benchmark experiments.

Type	Overall volume, cm^3	Dimension, cm			Average density, g/cm^3
		a	b	c	
I	$9.52 \cdot 10^4$	5.08	5.08	5.08	1.833
II		5.08	5.08	10.16	1.845
III		5.08	5.08	2.54	

Chemical analysis, obtained from the manufacturing company as a sample from the inventory, which is may not be representative, is given in Table 4.

Table 4 Beryllium sample chemical composition.

Chemical composition	Content
Be, %	98.82
BeO, %	1.13
C, ppm	840
Fe, ppm	1250
Al, ppm	710

In addition to impurities mentioned in Table 4, beryllium contains unspecified impurities with a total amount of less than 400 ppm [8]. The composition of these impurities may contain elements, such as Li, B, Cd and others, which can affect the distribution of thermal neutrons, due to the parasitic absorption of thermal neutrons in the beryllium material.

Sample and integral analyses were completed in order to gain information on unspecified impurities. Sample analysis was completed by the ICP-MS method, and integral analysis – by the neutron pulsed method. Results obtained in these analyses are in a reasonably good agreement and are described in detail in the reference [9]. Detailed chemical composition of the sample is presented in Table 5. Some of the elements were detected, though their quantities were not measured absolutely (such elements are indicated by symbol "S").

Table 5 Chemical composition of the S-200-F standard grade beryllium measured with the ICP-MS method.

Element	Content	Element	Content
Be, %	97.9±0.8	Ni, ppm	250±30
Li, ppm	< 1	Zr	S
B, ppm	< 3	Nb	S
Mg, ppm	110±5	Mo	S
Al, ppm	570±50	Cd, ppm	< 1
Sc	S	Dy	S
Ti	S	Ta	S
V	S	W	S
Cr	S	Hg	S
Mn, ppm	96±5	Pb	S
Fe, ppm	1300±70	Th, ppm	1.5±0.1
Co	S	U, ppm	82±3

It has been experimentally proven by the neutron pulsed method [9], that effective absorption of thermal neutrons in beryllium used for construction of the blanket mock-up is approximately 30% higher than the calculated value, based on the data specified by the manufacturing company.

4.2.3. Tungsten, Ferritic and Stainless Steels

Tungsten plates were used to simulate armor material of the fusion reactor plasma facing components. All the plates were formed with dimensions of 50 x 50 mm and thicknesses varying from 5 to 25 mm. The chemical composition is presented in Table 6.

Table 6 Chemical composition of tungsten.

Element	Content, wt%
W	94.8±0.2
Ni	3.1±0.1
Cu	2.1±0.1

The tungsten density is 17.9±0.1 g/cm^3.

Low activation ferritic steel F82H was developed in Japan for application in the future fusion reactor [10]. The developed ferritic steel material was used in present integral experiments in order to simulate the structural material of the first wall. Steel plates with a thickness of 16 mm and sizes varying from 200x200 to 50x50 mm, were used to assemble the layer. Steel specifications are given in Table 7.

Table 7 Chemical composition of ferritic steel, F82H.

Element	Content, wt%	Element	Content, wt%
Fe	89.74	Cu	0.01
Cr	7.74	Ni	0.02
W	1.95	Mo	0.01
C	0.095	V	0.18
Si	0.1	Nb	0.0001
Mn	0.1	Ta	0.04
P	0.005	Ti	0.005
S	0.0031	B	1.496E-4

Type 316 stainless steel was used to manufacture the source reflector and the mock-up enclosure. The source reflector was manufactured in a hollow cylinder shaped form with a

back wall. The cylinder has an outer diameter of 1200 mm, an inner diameter of 800 mm, and a length of 609 mm. The back wall has a diameter of 1200 mm and a thickness of 203 mm. Since the target assembly of the neutron source had to be inserted to the cavity of the source reflector, an 80 x 160 mm hole was made in the centre of the back wall. Atomic number densities of SS316 are listed in Table 8.

Table 8 Chemical composition of type 316 stainless steel (SS316) used for the source reflector and mock-up enclosure.

Element	Density, $1/cm^3$	
	Source Reflector	Mock-up enclosure
C	$7.170 \cdot 10^{19}$	$1.988 \cdot 10^{20}$
Si	$9.444 \cdot 10^{20}$	$8.161 \cdot 10^{20}$
P	$4.316 \cdot 10^{19}$	$4.889 \cdot 10^{19}$
S	$1.878 \cdot 10^{18}$	$4.468 \cdot 10^{18}$
Cr	$1.548 \cdot 10^{22}$	$1.503 \cdot 10^{22}$
Mn	$9.796 \cdot 10^{20}$	$1.356 \cdot 10^{21}$
Fe	$5.759 \cdot 10^{22}$	$5.833 \cdot 10^{22}$
Ni	$9.713 \cdot 10^{21}$	$9.146 \cdot 10^{21}$
Mo	$1.050 \cdot 10^{21}$	$1.025 \cdot 10^{21}$

5. Experimental Techniques

5.1. Measurement of Tritium Production Rate using Diagnostic Pellets

In experiments on the blanket mock-up, the TPR measurements must meet the following requirements:

- ✓ accuracy;
- ✓ sensitivity;
- ✓ good spatial resolution;
- ✓ non-perturbation of the thermal neutron field.

Non-perturbation of the neutron field and a good spatial resolution are especially important for measurements of the local TPR inside the lithium-containing layer, due to the quick gradient of thermal neutron flux and appropriate distribution of tritium production (Fig. 2) in the vicinity of material (lithium titanate and beryllium) boundaries. Thus, at present, only the method based on activation of the diagnostic pellets inserted into the lithium layer can fully satisfy these requirements.

Evaluation of the TPR is derived by measuring tritium activity in the diagnostic pellet and the D-T neutron yield. Diagnostic pellets with a diameter of 13 mm and thicknesses of 0.5, 1.0 and 2.0 mm, were manufactured by cold pressing of the Li_2CO_3 powder and the respective pellet weight was: 0.105, 0.210 and 0.420 g. The lithium carbonate (Li_2CO_3) possesses several benefits, in which the most vital are:

- ✓ it is a well soluble and non-hydroscopic salt;
- ✓ in the process of irradiation of Li_2CO_3, tritium is generated and stored in the salt in chemical form of LiOT [11], therefore:
  - o presence of an insignificant chance to lose tritium before dissolution;
  - o stored tritium can be easily moved to solution;
- ✓ simple handling and fabrication process of the pellets.

Depending on intention, several pellet combinations with appropriate lithium isotope enrichment were used in the experiment. To measure the reaction rates on lithium isotopes for verification of neutron transport through the mock-up, a combination of pellets with lithium-7 (99.94%) and lithium-6 (A type) were used. In this case, in order to minimize the perturbation effect of thermal neutron flux in the beryllium, thin Li_2CO_3 pellets with a low enrichment of lithium-6 (A type) were selected. For measurement of tritium production rates in the lithium titanate layer, pellets were used with lithium-7 (99.94 %) and lithium-6 (T type) pellets. Absorption property of the pellets (T type) for the thermal neutrons was adjusted to the appropriate value of the surrounding lithium titanate material. Adjustment was performed by mixing fine powders with two lithium-6 enrichments: 7.55 and 95.5 %. Manufacturer information concerning the powder chemical and isotope compositions is presented in Table 9.

Table 9 Chemical composition of lithium carbonate powders used for the pellet fabrication

Element / Nuclide	Content		
	Natural enrichment	Lithium-6 enriched	Lithium-7 enriched
^{6}Li, atm %	7.552	95.616±0.005	0.057
^{7}Li, atm %	92.448±0.005	4.384	99.943±0.005
Na, ppm	0.2	< 50	< 2
Mg, ppm	0.06	< 5	< 1
Al, ppm	< 0.2	< 10	
S, ppm	< 7		
Cl, ppm	< 2		< 2
K, ppm	< 0.1	< 20	< 0.5
Ca, ppm	0.7	< 50	< 3
Ti, ppm	< 2		
Mn, ppm	< 0.1	< 10	
Fe, ppm	< 0.2	< 10	< 0.4
Ni, ppm	< 1	< 50	
Cu, ppm	< 0.01	< 5	< 1
Zr, ppm	< 2		
Mo, ppm	< 5		
Ba, ppm	< 20	< 5	< 20
Pb, ppm	< 0.02		< 7

The content of the main element in the fabricated pellets is shown in table 10.

Table 10 Chemical composition of lithium carbonate pellets depending on type.

Element / Nuclide	Density, 1/cm^3		
	^{6}Li (A type) (^{6}Li – 1.18%)	^{7}Li type (^{7}Li - 99.94%)	^{6}Li (T type) (^{6}Li – 43.88%)
^{6}Li	3.034E+20	1.697E+19	1.141E+22
^{7}Li	2.541E+22	2.570E+22	1.460E+22
C	1.285E+22	1.286E+22	1.301E+22
O	3.856E+22	3.857E+22	3.902E+22

Ahead of the irradiation procedure, pellets were wrapped into aluminum foil in order to avoid radioactive contamination from the surrounding medium.

Tritium activity produced in irradiated pellets was measured with a liquid scintillation spectrometer after the wet-chemistry treatment procedure. The binary acid method was utilized for the procedure (elaborately described in reference [12]). Briefly, utilizing the binary acid solvent for pellets and the surfactant-containing scintillation cocktail combination creates a very effective method, which meets requirements for design-oriented blanket experiments. The processing scheme of the method is shown in Fig. 8. A mixture of two acids, HNO_3 (61%) and CH_3COOH (100%), strong and weak acids, respectively, has been used as a binary acid solvent for the lithium carbonate pellet. The optimum acid volume ratio was determined by figure of merit and the sample compatibility in relation to the acid volume ratio and the pellet weight. In contrast with conventional techniques, all preprocessing procedures of the present method are performed in a standard scintillation vial, without the removal of lithium salts. Thus, this method is very simple and convenient, and at the same time it has the highest figure of merit.

The pellet solution was mixed with a commercially available cocktail - Clear-sol (Nakarai Chemical Co. Ltd., Japan). Tritium activity of the scintillation sample was measured with a scintillation spectrometer (Aloka 5100). The internal standard method was applied to evaluate the tritium counting efficiency. In the end, the tritium activity in the pellet was calculated according to the formula:

$$Q = \frac{C}{\varepsilon \cdot w \cdot f_d \cdot f_e \cdot f_g}, \tag{1}$$

where: Q – tritium activity (Bq/g);

C - net tritium count rate (1/sec);

ε - counting efficiency;

w - pellet weight (g);

f_d - correction factor for decay;

f_e - correction factor for triton escape;

f_g - correction factor for the tritium gaseous phase.

It is important to note, that an insignificant fraction of tritium produced in the pellet can be lost, due to a variety reasons. During irradiation of lithium pellets, tritons created around the surface boundary have a possibility to escape the pellet, due to the high kinetic energy. This fraction of lost tritium depends mainly on the size, chemical composition of the pellet and neutron energy. For the Li_2CO_3 pellet with a diameter of 13 mm and a thickness of 1.0 mm irradiated by thermal neutrons, the escape factor was about 2.5 % [13]. Another important fraction of lost tritium concerns the gaseous tritium phase produced during irradiation. This phase has a chance to be partly lost during irradiation or a subsequent chemical procedure. The phase depends on the fabrication procedure of pellets, their composition, and chemical treatment. For the Li_2CO_3 pellets fabricated by cold pressing, the factor was estimated to be 7 % [13].

Tritium activity produced in pellets, enriched by lithium-7, at the end of irradiation can be calculated by the following equation:

$$ {}^{7}Q = \left(RR_6 \cdot {}^{7}n_6 + RR_7 \cdot {}^{7}n_7\right) \cdot Y \cdot \lambda , \qquad (2) $$

where: ${}^{7}Q$ – tritium activity in the lithium-7 enriched pellet (Bq/g);

RR_6 and RR_7 – tritium production rate on the lithium-6 and 7 isotopes (1/Li nuclide/s.n.);

${}^{7}n_6$ and ${}^{7}n_7$ - isotopic density of lithium-6 and 7 in the pellet enriched by lithium-7, respectively (nuclide/g);

λ - decay constant for tritium (1/s);

Y – neutron source yield (neutrons).

In a similar manner, tritium activity produced in pellets enriched by lithium-6, at the end of irradiation can be calculated by the following equation:

$$ {}^{6}Q = \left(RR_6 \cdot {}^{6}n_6 + RR_7 \cdot {}^{6}n_7\right) \cdot Y \cdot \lambda \qquad (3) $$

Considering the linear equations (2) and (3) as simultaneous equations, tritium production rates, RR_6 and RR_7, were derived:

$$RR_6 = \frac{\left({}^6Q - {}^7Q \frac{{}^6n_7}{{}^7n_7} \right) \cdot \frac{1}{Y \cdot \lambda}}{{}^6n_6 - {}^7n_6 \frac{{}^6n_7}{{}^7n_7}}, \tag{4}$$

$$RR_7 = \frac{\left({}^7Q - {}^6Q \frac{{}^7n_6}{{}^6n_6} \right) \cdot \frac{1}{Y \cdot \lambda}}{{}^7n_7 - {}^6n_7 \frac{{}^7n_6}{{}^6n_6}}. \tag{5}$$

Table 11 lists several factors contributing to uncertainties of the measured tritium reaction rates.

Table 11 Sources and magnitudes of uncertainties in tritium production rate results.

Sources of uncertainty	Magnitude, %
Neutron yield	3
Number of target atoms	1
Counting efficiency	3.5
^{3}H labile fraction	5
Pellet weight	0,1
Irradiation, cooling and measuring time	0,1
Counting statistics	2
Half life	0,5

As a result, all contributing factors in the quadrature gave an uncertainty of about 7 % in tritium production rates.

5.2. Measurement of Activation Reaction Rate using Foils and Pellets

The activation technique has been used in integral experiments on the mock-up in order to provide the neutron spectrum indices for verification of transport calculations. The technique has the following advantages for the integral experiment:

- ✓ well established method;
- ✓ response of the activation detectors was tested and evaluated in the dosimetry file;
- ✓ detector is able to provide a good spatial resolution and a small perturbation effect on the neutron field.

Taking into account the experimental objective, an appropriate set of nuclear reactions was selected. Reactions are listed in Table 12.

Table 12 Dosimetry reactions.

Reaction	Half-life	Abundance, %	γ/β_{max} energy, keV	Branch ratio, %	Threshold, MeV
$^{93}Nb(n,2n)^{92m}Nb$	10.15 d	100	934.5	99.0	9
$^{27}Al(n,\alpha)^{24}Na$	15.02 h	100	1368.9	100	5
$^{7}Li(n,n'\alpha)^{3}H$	12.33 y	---	18.6	100	4
$^{32}S(n,p)^{32}P$	14.26 d	95.03	1710	100	3
$^{197}Au(n,\gamma)^{198}Au$	2.694 d	100	411.8	95.5	---
$^{31}P(n,\gamma)^{32}P$	14.26 d	100	1710	100	---
$^{6}Li(n,\alpha)^{3}H$	12.33 y	---	18.6	100	---

The $^{93}Nb(n,2n)^{92m}Nb$ was selected to measure the distribution of high energy neutrons from the source. The $^{27}Al(n,\alpha)^{24}Na$, $^{32}S(n,p)^{32}P$ and $^{7}Li(n,n'\alpha)^{3}H$ reactions were selected because of the sensitivity to fast neutrons with an energy of more that 3 MeV, (this energy range is important for tritium production on lithium-7). The $^{197}Au(n,\gamma)^{198}Au$, $^{31}P(n,\gamma)^{32}P$ and $^{6}Li(n,\alpha)^{3}H$ reactions were selected due to the sensitivity to thermal neutrons, which are responsible for tritium production on lithium-6. From the availability of materials containing a nuclide of the interest reaction, detectors were prepared using metal foils or pellets fabricated by cold pressing of powders. The Nb and Al foils had a size of 10 x 10 x 0.1 mm^3 and the gold foils - 5 x 5 x 0.001 mm^3. All the pellets were fabricated with a diameter of 13

mm and a thickness of 1.0 mm. A detailed description of activation detectors is shown in Table 13.

Table 13 The properties of activation detectors.

Reaction	Form / Material	Weight density, g/cm^3	Chemical composition	
			Element / Nuclide	Density, 1/cm^3
$^{93}Nb(n,2n)^{92m}Nb$	Foil / Nb	8.56	^{93}Nb	$5.49\cdot10^{22}$
$^{27}Al(n,\alpha)^{24}Na$	Foil / Al	2.71	Al	$6.04\cdot10^{22}$
$^{7}Li(n,n'\alpha)^{3}H$	Pellet / Li_2CO_3	1.58	6Li	$1.697\cdot10^{19}$
			7Li	$2.570\cdot10^{22}$
			C	$1.286\cdot10^{22}$
			O	$3.857\cdot10^{22}$
$^{32}S(n,p)^{32}P$	Pellet / $CH_3SO_2CH_3$	1.42	H	$5.45\cdot10^{22}$
			C	$1.82\cdot10^{22}$
			O	$1.82\cdot10^{22}$
			S	$9.09\cdot10^{21}$
$^{197}Au(n,\gamma)^{198}Au$	Foil / Au	19.28	Au	$5.89\cdot10^{22}$
$^{31}P(n,\gamma)^{32}P$	Pellet / $NH_4PH_2O_2$	1.45	H	$6.31\cdot10^{22}$
			N	$1.05\cdot10^{22}$
			O	$2.10\cdot10^{22}$
			P	$1.05\cdot10^{22}$
$^{6}Li(n,\alpha)^{3}H$	Pellet / Li_2CO_3	1.58	6Li	$3.034\cdot10^{20}$
			7Li	$2.541\cdot10^{22}$
			C	$1.285\cdot10^{22}$
			O	$3.856\cdot10^{22}$

Lithium carbonate, Li_2CO_3, was used for lithium-containing pellets. The technique for measurement of tritium activity in pellets is described in Chapter 5.1.

The compounds of $CH_3SO_2CH_3$ and $NH_4PH_2O_2$ were used to prepare sulfur- and phosphorous-containing pellets. These compounds were selected to enable measurements of ^{32}P activity in water by means of Cherenkov radiation counting. Such an approach has significantly improved the sensitivity and accuracy of analysis. The technique utilizes the principle of direct Cherenkov radiation counting of energetic β-rays in an aqueous medium. Cherenkov radiation produces a bluish light when β-particles of energy greater than 260 keV travel through a medium such as water. Since no scintillator is required and chemical quenching is absent, sample preparation is extremely simple and the technique is ideal for the assay of ^{32}P in aqueous solution. After irradiation the pellets were simply dissolved in water. Aqueous solutions were assayed in 20 ml opaque Teflon vials, which were found to yield a higher counting efficiency than low background glass vials, presumably due to diffusion of directional Cherenkov emissions. Counting efficiency was estimated with the internal standard method. The Cherenkov radiation counting technique is described in detail in the reference [14].

Gamma activities of irradiated foils were measured by a standard technique with the Ge detector. The interest reaction rate was derived from an appropriate count rate according to the formula:

$$RR = \frac{\lambda \cdot C \cdot A}{w \cdot \varepsilon \cdot a \cdot b \cdot Y \cdot f_c \cdot \mu \cdot N_A \cdot (1-\exp(-\lambda \cdot t_i)) \cdot \exp(-\lambda \cdot t_c) \cdot (1-\exp(-\lambda \cdot t_m))}, \qquad (6)$$

where:

λ - decay constant,

C - counts, (1/sec),

A - atomic mass,

ε - counting efficiency,

N_A - Avogadro's number,

A - abundance of the target element,

b - branching ratio,

Y - neutron source strength (1/sec),

f_c - correction factor for the decay during irradiation,

μ - self absorption correction factor,

t_i, t_c, t_m - irradiation, cooling and collection time, respectively.

The f_c factor was estimated based on the neutron yield monitor data. Major sources of uncertainty for the reaction rate are listed in Table 14.

Table 14 Estimated maximum uncertainties for the measured reaction rate

Sources of uncertainty	**Magnitude, %**
Neutron yield	3
Efficiency of γ-detector	3
Counting statistics	1
Number of target atoms	0.2
Pellet weight	0,1
Irradiation, cooling and measuring time	0,1
Decay data	0,5

Summing up all contributing factors in quadrature produced an uncertainty of about 5 % in reaction rates.

6. Experiment on the Blanket Mock-up Irradiated by Neutrons from the D-T Source

6.1. Experimental Configuration and Irradiation

The integral experiment was performed in the first target room at the FNS facility in JAERI. The facility provides good experimental conditions in regards to the neutron background, due to the large size of the target room (15 x 15 x 12 m^3). The blanket mock-up was located in front of the neutron source at a distance of 448 mm from the target. In order to produce D-T neutrons, a target with a tritium activity of approximately $3.7 \cdot 10^{11}$ Bq was bombarded by a deuteron beam with an energy of 350 keV and an intensity of 1 mA at the target. The neutron yield was determined by the associated alpha-particle detector [15] with

an accuracy of 3 %. The neutron spectrum of the D-T source was comprehensively evaluated during early research [16].

Experimental configuration is shown in Fig. 9. The diagnostic pellets for tritium production rate measurements and activation detectors were inserted into the mock-up during construction. The pellet and foil arrangements are shown in Fig. 5 and 6. Irradiation of the blanket mock-up was performed for three days, ten hours per day, with a total neutron yield of $1.11 \cdot 10^{16}$ neutrons. After irradiation, pellets and foils were picked up from the mock-up and measured with appropriate techniques.

6.2. Results

In order to obtain a detailed distribution of the tritium production rate inside the lithium titanate layer with a thickness of 12 mm, 15 diagnostic pellets with a thicknesses varying from 0.5 to 2.0 mm were stacked together, with a total thickness of 12 mm, and inserted into the layer, Fig. 7. Experimental data of the tritium production rate via the $^{6}Li(n,\alpha)^{3}H$ reaction inside the breeding layer is shown in Figure 10 and summarized in Table 15. The data enables us to conclude that the tritium production rate has changed drastically, about 20 times within the 12 mm layer, due to absorption of thermal neutrons by the ^{6}Li isotope. Several reaction rate distributions (such as $^{93}Nb(n,2n)^{92m}Nb$, $^{7}Li(n,n`\alpha)^{3}H$, $^{32}S(n,p)^{32}P$, $^{31}P(n,\gamma)^{32}P$) were measured in the mock-up. The first three reactions are sensitive to fast neutrons, while the last reaction – to thermal neutrons. Figures 11 and 12 show reaction distributions along the axis and table 16 summarizes the data. Reaction rates of threshold reactions give a similar trend in the mock-up. From Fig. 12 and 10, it may be seen that the distributions of $^{31}P(n,\gamma)^{32}P$ and $^{6}Li(n,\alpha)^{3}H$ reaction rates are similar inside the lithium titanate layer.

7. Experiment on the Blanket Mock-up Irradiated by Neutrons from the D-T Source with a Reflector

7.1. Impact of the Source Reflector on TPR

In the DEMO fusion reactor the neutron spectrum incoming to the blanket contains two components: high energy neutrons from D-T plasma, and low energy neutrons reflected at the

opposite side of the reactor vacuum chamber. In integral experiments on the blanket mock-up with the point D-T source, some simulation of the neutron environment can be done by surrounding the source with a reflector constructed with appropriate materials. The source reflector will drastically increase the number of low energy neutrons that enter the tested mock-up and, consequently, it will increase tritium production in layers that are close to the first wall. Therefore, to gain experimental data for verification, the second experiment on the blanket mock-up irradiated by neutrons from the D-T source with a reflector was completed.

The source reflector, which was used in the present experiment, was originally proposed for FNS bulk shielding experiments [17], with two targets in mind: reduction of the background with room returned neutrons, and an increase in the number of low energy neutrons, entering the tested shielding region. It is possible to consider such an experimental arrangement as an option for creating a simulation of a fusion reactor neutron environment, especially for shielding experiments, due to large shielding design margins. However, blanket design margins are much more severe, when compared to shielding design margins, and thus, simulation of the fusion reactor spectrum for the blanket experiments requires criteria other, than was used for shielding experiments. Lastly, the source reflector for simulation of the fusion reactor neutron environment, especially in the present experimental arrangement, can be considered as a simulation case.

The impact of the source reflector on the tritium production rate was estimated by calculations for the selected experimental arrangement. Calculation results are shown in Fig. 13. It was concluded that introduction of the source reflector will increase the TPR-6 by more than two times in the lithium titanate layer.

7.2. Experimental Configuration and Irradiation

The experimental configuration for the second integral experiment is shown in Fig. 14. In order to directly compare integral experiments with and without the source reflector, the second experiment was executed in the exactly same manner as the experiment without a source reflector. Additional foils were introduced outside the lithium titanate layer, for measurement of $^{27}Al(n,\alpha)^{24}Na$ and $^{197}Au(n,\gamma)^{198}Au$ reaction rates. The foils were attached to beryllium block surfaces in the same manner as pellets. Irradiation of the blanket mock-up

was performed for three days, ten hours per day with a total neutron yield of $9.98 \cdot 10^{15}$ neutrons.

7.3. Results

The experimental data of tritium production rate via the $^{6}Li(n,\alpha)^{3}H$ reaction inside the breeding layer is shown in Fig. 15 and summarized in Table 17. It appears that the tritium production rate gradient through the layer is less compared to the experiment without a reflector, due to a higher contribution of low-energy neutrons from the reflector. The data of reaction rates (such as $^{93}Nb(n,2n)^{92m}Nb$, $^{27}Al(n,\alpha)^{24}Na$ and $^{32}S(n,p)^{32}P$, which are sensitive to fast neutrons) are summarized in Table 18, and the distributions are shown in Fig. 16. Distributions show an adequate tendency of fast neutron behavior inside the blanket mock-up, where fast neutrons decrease according to their energy thresholds. Reaction rates of $^{197}Au(n,\gamma)^{198}Au$ and $^{31}P(n,\gamma)^{32}P$, which are sensitive to slow neutrons, are summarized in Table 18 and Fig. 17. These reactions show an opposite tendency, since the number of slow neutrons increases inside the mock-up. The $^{197}Au(n,\gamma)^{198}Au$ reaction rate was measured with and without the Cd cover. By comparing the data around the lithium titanate layer it is possible to conclude, that this reaction is activated mainly by epithermal neutrons. The contribution of thermal neutrons to activation of the $^{31}P(n,\gamma)^{32}P$ reaction is more significant, than can be seen from comparison of distributions in Fig. 17. From this comparison, it is possible to conclude that the $^{31}P(n,\gamma)^{32}P$ reaction is more useful for analysis of the neutron field in regards to the tritium production rate.

8. Experiment on the Blanket Mock-up with a Tungsten Armor Layer Irradiated by Neutrons from the D-T Source with a Reflector

8.1. Impact of the Armor Layer on TPR

The impact of tungsten armor on tritium production in the fusion reactor blanket was studied in detail in the reference [5]. This effect was estimated for the present experimental arrangement (data presented in Fig. 18). It was concluded, that placement of a tungsten layer

with a thickness of 25 mm before the ferritic steel layer will decrease the TPR via the $^{6}Li(n,\alpha)^{3}H$ reaction in the lithium titanate layer by 6 % at the most.

8.2. Experimental Configuration and Irradiation

In order to enhance the impact of the tungsten armor layer on the tritium production rate in the lithium titanate layer of the blanket mock-up, a layer with a thickness of 25.2 mm was selected. The layer was installed before the F82H layer. An experimental configuration for the third integral experiment is shown in Fig. 19. To directly compare all three integral experiments, the third experiment was performed identically to previous experiments. The set of foils and pellet detectors was the same as in the second experiment. Irradiation of the blanket mock-up was performed for three days, ten hours per day with a total neutron yield of $1.34 \cdot 10^{16}$ neutrons.

8.3. Results

The distributions of the measured activation reactions have the same tendencies as was observed in the second experiment. Experimental data of tritium production rate via the $^{6}Li(n,\alpha)^{3}H$ reaction inside the breeding layer is presented in Fig. 20 and summarized in Table 19. The reaction rate data of $^{93}Nb(n,2n)^{92m}Nb$, $^{27}Al(n,\alpha)^{24}Na$, $^{7}Li(n,n'\alpha)^{3}H$ and $^{32}S(n,p)^{32}P$, which are sensitive to fast neutrons, are summarized in Table 20, and appropriate distributions are shown in Fig. 21. The reaction rates of $^{197}Au(n,\gamma)^{198}Au$ and $^{31}P(n,\gamma)^{32}P$, which are sensitive to slow neutrons, are summarized in Table 20 and Fig. 22.

9. Comparison between Integral Experiments

Experimental data acquired in integral experiments on the blanket mock-up was compared in order to estimate the impact of a source reflector and the tungsten armor layer on the tritium production rate and the distributions of fast and slow neutrons.

The integrated datum of tritium production rates along the central axis of the mock-up is summarized in Table 21 and the distributions are presented in Fig. 23.

Table 21 Comparison of tritium production via the $^{6}Li(n,\alpha)^{3}H$ reaction along the center axis in the lithium titanate layer for integral experiments

	Experimental configuration		
	Without Source Reflector and Tungsten layer	With Source Reflector	
		With Tungsten layer	Without Tungsten layer
Relative Tritium Production	1.0	2.04	2.18
	---	0.94	1.0

Results indicate that the source reflector significantly increases the tritium production (by about 2.2 times), and the tungsten layer with a thickness of 25.2 mm slightly decreases the rate (by about 6 %). A similar tendency is seen for distribution of thermal neutrons in the mock-up (Fig. 24).

Impact of the source reflector and the tungsten armor on distribution of fast neutrons in the mock-up depends on the reaction energy threshold. Experimental data comparisons are shown in Fig. 25, 26. In the experiment with and without a source reflector, no difference exists for distributions of the $^{93}Nb(n,2n)^{92m}Nb$ reaction rate (E_{Thres} ~ 9 MeV), and an insignificant increase of less that 10 % around the breeder layer exists for the $^{32}S(n,p)^{32}P$ (E_{Thres} ~ 2 MeV) reaction rate. Introduction of the tungsten layer decreased the reaction rates for fast neutrons by more than 20 %.

General data observations for activation reactions in experiments with and without the source reflector show that the ratio of appropriate reaction rates is the largest on the front surface of the mock-up and have a tendency to decrease inside the mock-up.

10. Example of Experimental Analysis

10.1. Nuclear Data and the Transport Calculation Code

The continuous energy Monte-Carlo transport code MCNP-4C was used to calculate the reaction rates of interest. The Japanese Evaluated Nuclear Data Library JENDL-3.2 and JENDL Dosimetry File were used for the calculation.

10.2. Results

Experimental data gained in the experiment on the mock-up irradiated by neutrons from the D-T source was compared with appropriately calculated values for the $^{92}Nb(n,2n)^{92m}Nb$, $^{32}S(n,p)^{32}P$ and $^{6}Li(n,\alpha)^{3}H$ reactions. Calculated to experimental rate ratios for $^{92}Nb(n,2n)^{92m}Nb$ and $^{32}S(n,p)^{32}P$ reactions show a reasonable agreement within estimated uncertainties (Fig. 27 – 28). Based on these results, it is possible to conclude that the neutron transport calculation for neutrons with energy of above 2 MeV can predict the reaction rate. This observation is also valid for tritium production via the $^{7}Li(n,n`\alpha)^{3}H$ reaction, whose energy threshold is more than 3.8 MeV and the neutron sensitivity is similar to the $^{32}S(n,p)^{32}P$ reaction. A reasonable agreement between experimental and calculated results exists for tritium production via $^{6}Li(n,\alpha)^{3}H$ reaction, Fig. 29. The appropriate ratio of calculated to experimental TPR was approximately 1.02. Comparison of calculated and experimental results indicated that the TPR could be predicted by calculation within estimated uncertainties.

Analysis of experimentally obtained data on the mock-up with and without the tungsten layer irradiated by neutrons from the D-T source with a reflector shows a reasonable agreement with the calculated values for $^{92}Nb(n,2n)^{92m}Nb$ and $^{32}S(n,p)^{32}P$ reactions, (Fig. 30 - 31). Analysis of the tritium production rate shows that the calculated data has overestimated the measured data (Fig. 32). The observation is valid for experiments on the blanket mock-up with and without the tungsten layer. The average ratio of calculated to experimental TPR values was about 1.14 for the experiment without a tungsten layer, and 1.11 – for the experiment with a tungsten layer. It was previously discussed, that the source reflector drastically changes the incoming neutron spectrum for blanket mock-up with an increase in the tritium production rate by more that two times. Thus, one of the possible reasons for the observed overestimation in the experiment with the source reflector is an inadequate description of backward scattering contribution of neutrons from the SS316 source reflector. Appropriate nuclear data should be reevaluated in order to improve reactor design calculations.

11. Conclusions

The first series of integral experiments was performed on the blanket mock-up containing F82H, lithium titanate and beryllium layers, with respective thicknesses of 16 mm, 12 mm and 203 mm. The study focused on verification of tritium production. Three integral experiments were executed on the blanket mock-up in order to study the impact of the tungsten armor and the incoming neutron spectrum on the tritium production. Direct measurements of the tritium production rate were performed using diagnostic pellets inserted into the breeder layer. Distribution of tritium production rate inside the lithium titanate layer was measured with a spatial resolution of 0.5 mm. Obtained experimental data allows to study the tritium production rate heterogeneous effect around the boundary between the lithium titanate and beryllium layers.

The first integral experiment was performed on the blanket mock-up irradiated by neutrons from the D-T source. Analysis showed that the tritium production rate in the lithium titanate layer can be predicted adequately to experimental values. Obtained calculation to experimental ratio equals 1.02.

In the second experiment, the incoming neutron spectrum was changed with the SS316 steel made source reflector. The source reflector drastically increases the number of low-energy neutrons incoming to the mock-up and appropriately increases tritium production in the breeder layer by more than two times compared with an experiment without a source reflector. Analysis showed that calculation of the tritium production rate via the $^{6}Li(n,\alpha)^{3}H$ reaction overestimated the experimental value by a factor of 1.14. One of the overestimation reasons may be the inadequate description of the contribution of backward scattering neutrons from the source reflector.

In the third experiment, the tungsten layer was placed in front of the mock-up and irradiated by neutrons from the D-T source with a reflector. In order to enhance the tungsten armor effect, a tungsten layer with a thickness of 25.2 mm was used in the experiment. Introduction of the layer decreased the tritium production by 6 %. Analysis of the calculated to experimental ratios showed results quite similar to data obtained in the second experiment. Calculation of the tritium production rate via the $^{6}Li(n,\alpha)^{3}H$ reaction overestimated the experimental value by a factor of 1.12.

Finally, based on the data gained in the study, it is necessary to emphasize several points. In the DEMO fusion reactor, the neutron spectrum incoming to the blanket contains two components: high-energy neutrons from the D-T plasma, and low energy neutrons, reflected at the opposite side of the reactor vacuum chamber. The stated situation was simulated in two integral experiments on the blanket mock-up irradiated by neutrons from the D-T source with and without a reflector. Obtained results have demonstrated the importance of an adequate description of backward scattering neutrons for accurate tritium breeding prediction in layers located near the first wall of the blanket.

Acknowledgments

The authors gratefully acknowledge C. Kutsukake, S. Tanaka, Y. Abe, M. Seki and Y. Oginuma, for their excellent operation of the D-T neutron source at the FNS facility.

References

[1] Phase IIA and IIB Expeirments of JAERI/U.S.DOE Collaborative Program on Fusion Blanket Neutronics, Ed. Y. Oyama, Japan Atomic Energy Research Institute Report, JAERI-M 89-215 (1990).

[2] V. V. Afanas'ev, A.G. Belevitin, Yu. M. Verzilov, V. L. Romodanov, D. V. Markovskiy, G. E. Shatalov, "Experiment on the Hybrid Blanket Model with Uranium Multiplier", Proceedings of the XIX International Symposium on the Nuclear Physics, Gaussig, Germany, November 6 -10, 1989, 34-38 (1990).

[3] S. Konishi, S. Nishio and K. Tobita, The DEMO design team, "DEMO plant design beyond ITER", Fusion Engin. Des. 63-64, 11-17 (2003).

[4] M. Enoeda, Y. Kosaku, T. Hatano, T. Kuroda, N. Miki, T. Honma, and M. Akiba, "Design and technology development of solid breeder blanket cooled by supercritical water in Japan", FT/P1-08, Fusion Energy 2002 (Proc. 19th Fusion Energy Conference, Lyon, 2002) (Vienna IAEA), CD-ROM file FT/P1-08, http://www.iaea.org/programmes/ripc/physics/fec2002/html/fec2002.htm.

[5] S. Sato, T. Nishitani, "Impact of armor materials on tritium breeding ratio in the fusion reactor blanket", J. Nuclear Materials, 313-316, 690-695 (2003).

[6] Y. Yanagi, S. Sato, M. Enoeda, T. Hatano, S. Kikuchi, T. Kuroda, Y. Kosaku and Y. Ohara, "Nuclear and Thermal Analyses of Supercritical-water-cooled Solid breeder Blanket for Fusion DEMO Reactor", J. Nucl. Sci. Tech., 38, 1014-1018 (2001).

[7] M. Ito, JAERI, private communication (2003).

[8] D. E. Dombrowski, "Manufacture of beryllium for fusion applications", Fusion Eng. Des. 37, 229-242 (1997).

[9] Y.Verzilov, K. Ochiai, S. Sato, M. Wada, M. Yamauchi, T. Nishitani, "Analysis of Impurities in Beryllium, affecting Evaluation of the Tritium Breeding Ratio", JAERI-Research 2004-005 (2004).

[10] A. Kohyama, A. Hishinuma, D.S. Gelles, R.L. Klueh, W. Dietz and K. Ehrlich, "Low-activation ferritic and martensitic steels for fusion application", J. Nucl. Mater., 138-147, 233 (1996).

[11] H. Kudo, K. Tanaka, H. Amano, "Chemical Behaviors of Tritium Produced by the $^{6}Li(n,\alpha)^{3}H$ reaction in Lithium Oxide", J. Inorg. Nucl. Chem., 40, 363 (1978).

[12] Y. Verzilov, F. Maekawa, Yu. Oyama, "A Novel Method for Solving Lithium Carbonate Pellet by Binary-Acid for Tritium Production Rate Measurement by Liquid Scintillation Counting Technique", J. Nucl. Sci. Techn., 33, 390-395 (1996).

[13] Y. Verzilov, V.V. Afanasev, A.G. Belevitin, M.A. Ziganov, V.L. Romodanov, "Tritium Loss at Neutron Irradiation Detector Contained Lithium", Vopr. Atom. Nauki Techniki, (in Russian), Vol.2, 53 (1990).

[14] Y. Verzilov, F. Maekawa, Yu. Oyama, Y. Ikeda, "Measurements of the $^{32}S(n,p)^{32}P$ and $^{35}Cl(n,\alpha)^{32}P$ Reaction Cross Sections in the Energy Range of 13.3 - 14.9 MeV and their Integral Test below 14 MeV", Fusion Eng. Des., 37, 95 - 105 (1997).

[15] H. Maekawa, Y. Ikeda, Y. Oyama, S. Yamaguchi and T. Nakamura, "Neutron Yield Monitors for the Fusion Neutronic Source (FNS) ---For 80^0 Beam Line---", Japan Atomic Energy Research Institute Report, JAERI-M 83-219 (1983).

[16] F. Maekawa, C. Konno, K. Kosako, Y. Oyama, Y. Ikeda and H. Maekawa, "Bulk Shielding Experiments on Large SS316 Assemblies Bombarded by D-T neutrons. Volume II: Analysis", Japan Atomic Energy Research Institute Report, JAERI-Research 94-044 (1994).

[17] C. Konno, F. Maekawa, A. Iwai, K. Kosako, Y. Ikeda, Y. Oyama and H. Maekawa, "Pre-analyses of SS316 and SS316/Water Bulk Shielding Experiments", Japan Atomic Energy Research Institute Report, JAERI-Tech 94-019 (1994).

[18] T. Nakagawa, H. Kawasaki, K. Shibata (Eds.), "Curves and Tables of Neutron Cross Sections in JENDL −3.3", Japan Atomic Energy Research Institute Report, JAERI-Data/Code 2002-020 (2002).

Table 15. Measured tritium production rate via the $^{6}Li(n,\alpha)^{3}H$ reaction in the lithium titanate layer of the blanket mock-up irradiated by neutrons from the D-T source

Distance from the surface of the lithium titanate layer, mm	Tritium production rate, 1/^{6}Li nuclide/s.n.	Absolute error
0.25	2.25E-28	1.55E-29
0.75	2.27E-28	1.57E-29
1.50	2.32E-28	1.60E-29
2.50	2.40E-28	1.66E-29
3.50	2.49E-28	1.72E-29
4.50	2.71E-28	1.87E-29
5.50	2.98E-28	2.05E-29
7.00	3.72E-28	2.57E-29
8.50	5.30E-28	3.66E-29
9.25	6.80E-28	4.70E-29
9.75	8.95E-28	6.17E-29
10.25	1.23E-27	8.47E-29
10.75	1.72E-27	1.19E-28
11.25	2.63E-27	1.82E-28
11.75	4.76E-27	3.29E-28

Table 16. Measured activation reaction rates in the blanket mock-up irradiated by neutrons from the D-T source

Distance from the front surface of the mock-up, mm	$^{93}Nb(n,2n)^{92m}Nb$		$^{32}S(n,p)^{32}P$		$^{31}P(n,\gamma)^{32}P$	
	Reaction rate, 1/nuclide/s.n.	Absolute error	Reaction rate, 1/nuclide/s.n.	Absolute error	Reaction rate, 1/nuclide/s.n.	Absolute error
-0.5	1.93E-29	9.48E-31	1.19E-29	5.97E-31	1.08E-31	5.38E-33
16.5	1.54E-29	7.55E-31	1.10E-29	5.48E-31	1.46E-31	7.28E-33
29.5	1.34E-29	6.58E-31	1.06E-29	5.32E-31	1.89E-30	9.46E-32
55.9	1.06E-29	5.19E-31	9.57E-30	4.79E-31	6.66E-30	3.33E-31
82.3	8.29E-30	4.07E-31	8.03E-30	4.01E-31	1.03E-29	5.16E-31

Table 17. Measured tritium production rate via the $^{6}Li(n,\alpha)^{3}H$ reaction in the lithium titanate layer of the blanket mock-up irradiated by neutrons from the D-T source with a reflector

Distance from the surface of the lithium titanate layer, mm	Tritium production rate, 1/^{6}Li nuclide/s.n.	Absolute error
0.25	7.18E-28	4.96E-29
0.75	7.12E-28	4.91E-29
1.50	7.15E-28	4.94E-29
2.50	7.27E-28	5.01E-29
3.50	7.53E-28	5.19E-29
4.50	7.71E-28	5.32E-29
5.50	8.10E-28	5.59E-29
7.00	9.51E-28	6.56E-29
8.50	1.22E-27	8.44E-29
9.25	1.64E-27	1.13E-28
9.75	1.92E-27	1.33E-28
10.25	2.24E-27	1.54E-28
10.75	3.09E-27	2.13E-28
11.25	4.71E-27	3.25E-28
11.75	9.06E-27	6.25E-28

Table 18. Measured activation reaction rates in the blanket mock-up irradiated by neutrons from the D-T source with a reflector

Distance from the front surface of the mock-up, mm	$^{93}Nb(n,2n)^{92m}Nb$		$^{27}Al(n,\alpha)^{24}Na$		$^{32}S(n,p)^{32}P$	
	Reaction rate, 1/nuclide/s.n.	Absolute error	Reaction rate, 1/nuclide/s.n.	Absolute error	Reaction rate, 1/nuclide/s.n.	Absolute error
-0.5	1.95E-29	9.55E-31			1.36E-29	6.79E-31
16.5	1.54E-29	7.57E-31	3.59E-30	1.80E-31	1.21E-29	6.07E-31
29.5	1.36E-29	6.68E-31	3.26E-30	1.63E-31	1.15E-29	5.76E-31
55.9	1.05E-29	5.17E-31			1.01E-29	5.05E-31
128			1.29E-30	6.47E-32		

Distance from the front surface of the mock-up, mm	$^{31}P(n,\gamma)^{32}P$		$^{197}Au(n,\gamma)^{198}Au$		$[^{197}Au(n,\gamma)^{198}Au]_{Cd}$	
	Reaction rate, 1/nuclide/s.n.	Absolute error	Reaction rate, 1/nuclide/s.n.	Absolute error	Reaction rate, 1/nuclide/s.n.	Absolute error
-0.5	4.05E-31	2.02E-32	1.72E-27	8.59E-29	1.73E-27	8.66E-29
16.5	4.38E-31	2.19E-32	1.57E-27	7.83E-29	1.51E-27	7.53E-29
29.5	3.41E-30	1.71E-31	5.51E-27	2.75E-28	4.63E-27	2.31E-28
55.9	1.18E-29	5.91E-31				
128			2.67E-26	1.34E-27	1.50E-26	7.50E-28

Table 19. Measured tritium production rate via the $^{6}Li(n,\alpha)^{3}H$ reaction in the lithium titanate layer of the blanket mock-up with W layer irradiated by neutrons from the D-T source with a reflector

Distance from the surface of the lithium titanate layer, mm	Tritium production rate, $1/^{6}Li$ nuclide/s.n.	Absolute error
0.25	7.01E-28	4.84E-29
0.75	6.97E-28	4.81E-29
1.50	6.86E-28	4.73E-29
2.50	6.91E-28	4.77E-29
3.50	7.26E-28	5.01E-29
4.50	7.53E-28	5.20E-29
5.50	7.98E-28	5.50E-29
7.00	9.53E-28	6.57E-29
8.50	1.16E-27	8.03E-29
9.25	1.48E-27	1.02E-28
9.75	1.81E-27	1.25E-28
10.25	2.19E-27	1.51E-28
10.75	2.96E-27	2.04E-28
11.25	4.41E-27	3.04E-28
11.75	7.91E-27	5.46E-28

Table 20. Measured activation reaction rates in the blanket mock-up with W layer irradiated by neutrons from the D-T source with a reflector

Distance from the front surface of the mock-up, mm	$^{93}Nb(n,2n)^{92m}Nb$		$^{27}Al(n,\alpha)^{24}Na$		$^{32}S(n,p)^{32}P$	
	Reaction rate, 1/nuclide/s.n.	Absolute error	Reaction rate, 1/nuclide/s.n.	Absolute error	Reaction rate, 1/nuclide/s.n.	Absolute error
-0.5	1.44E-29	7.09E-31	3.22E-30		1.06E-29	5.30E-31
16.5	1.09E-29	5.37E-31	2.53E-30	1.27E-31	8.97E-30	4.49E-31
29.5	9.56E-30	4.69E-31	2.40E-30	1.20E-31	8.52E-30	4.26E-31
55.9	7.48E-30	3.67E-31			7.34E-30	3.67E-31
128			8.74E-31	4.37E-32		

Distance from the front surface of the mock-up, mm	$^{31}P(n,\gamma)^{32}P$		$^{197}Au(n,\gamma)^{198}Au$		$[^{197}Au(n,\gamma)^{198}Au]_{Cd}$	
	Reaction rate, 1/nuclide/s.n.	Absolute error	Reaction rate, 1/nuclide/s.n.	Absolute error	Reaction rate, 1/nuclide/s.n.	Absolute error
-0.5	4.06E-31	2.03E-32	9.99E-28	5.00E-29	8.96E-28	4.48E-29
16.5	4.36E-31	2.18E-32	1.45E-27	7.25E-29	1.43E-27	7.14E-29
29.5	3.16E-30	1.58E-31	3.91E-27	1.95E-28	2.76E-27	1.38E-28
55.9	1.07E-29	5.37E-31				
128			1.37E-26	6.85E-28	1.20E-26	6.02E-28

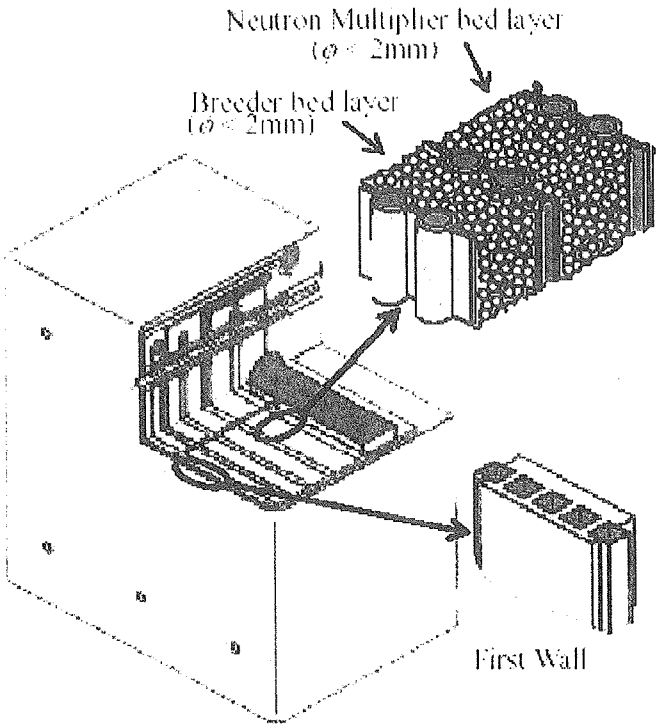

Figure 1. Structure of the DEMO Blanket Module.

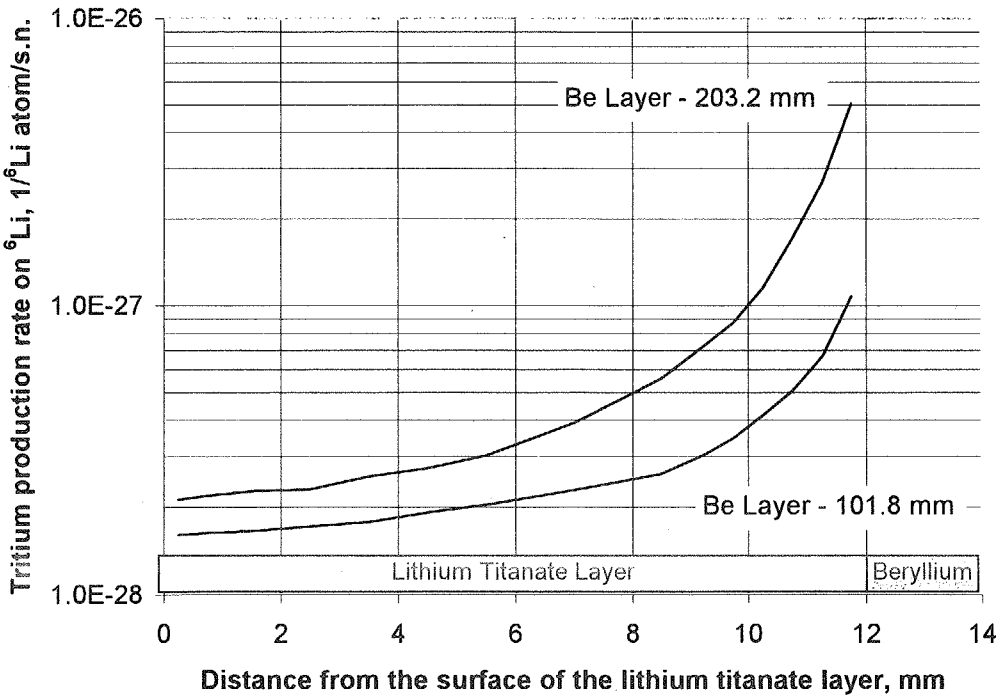

Figure 2. Distribution of TPR via $^6Li(n,\alpha)^3H$ reaction inside the lithium titanate layer for mock-up compositions with various beryllium layer thicknesses.

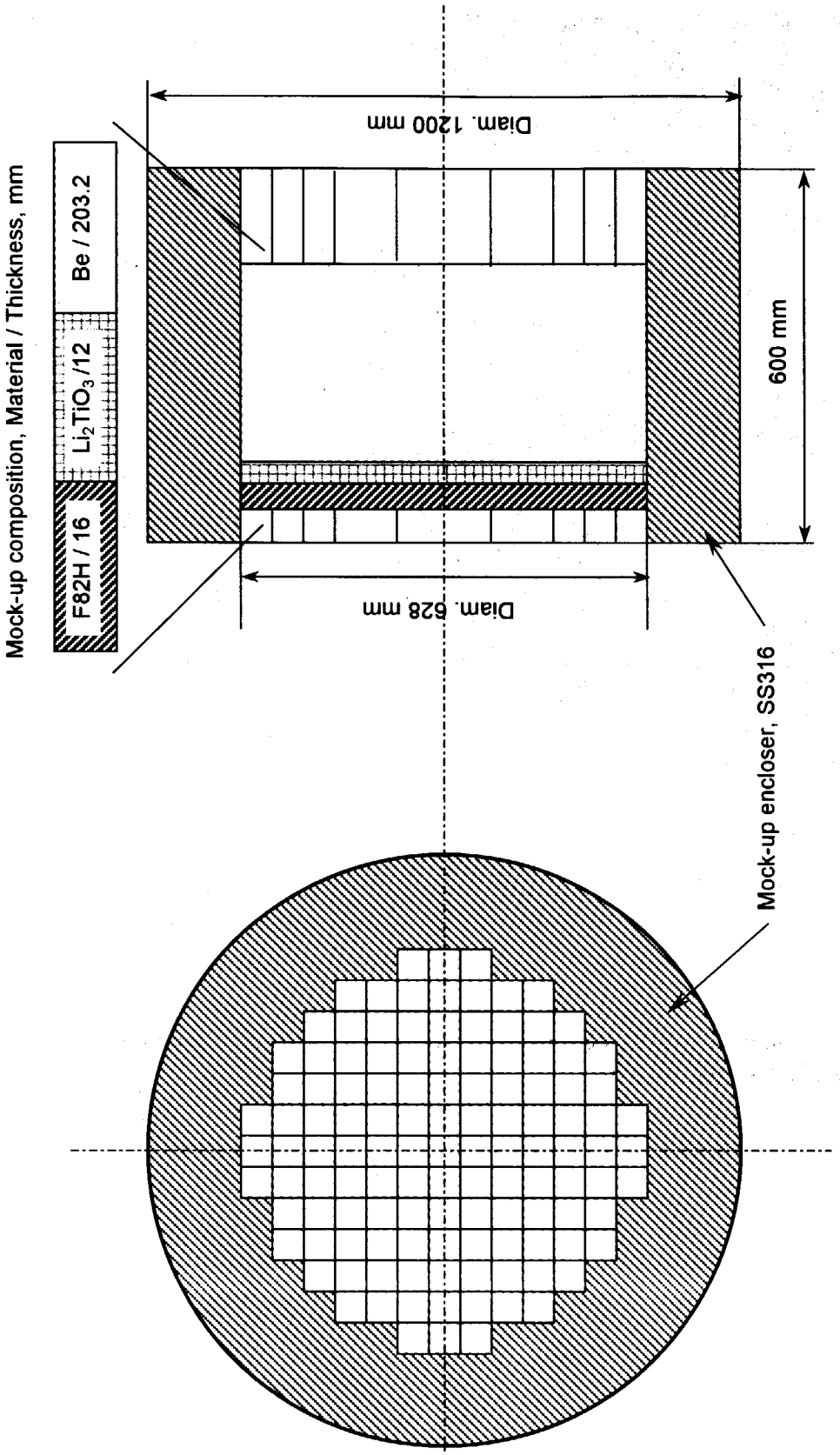

Figure 3. Basic arrangement of the blanket mock-up with a one breeder layer.

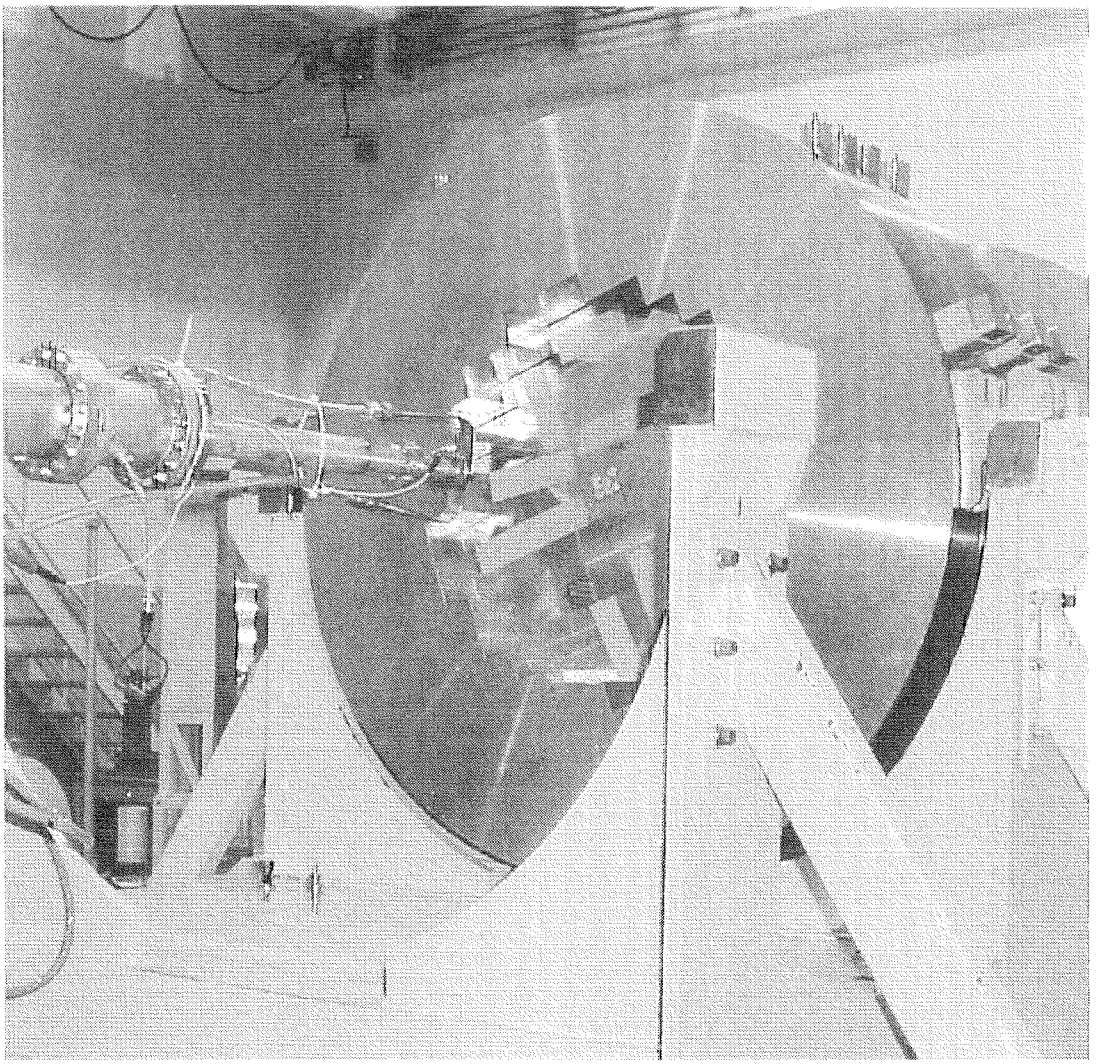

Figure 4. Experimental arrangement view of the blanket mock-up placed inside a stainless steel enclosure.

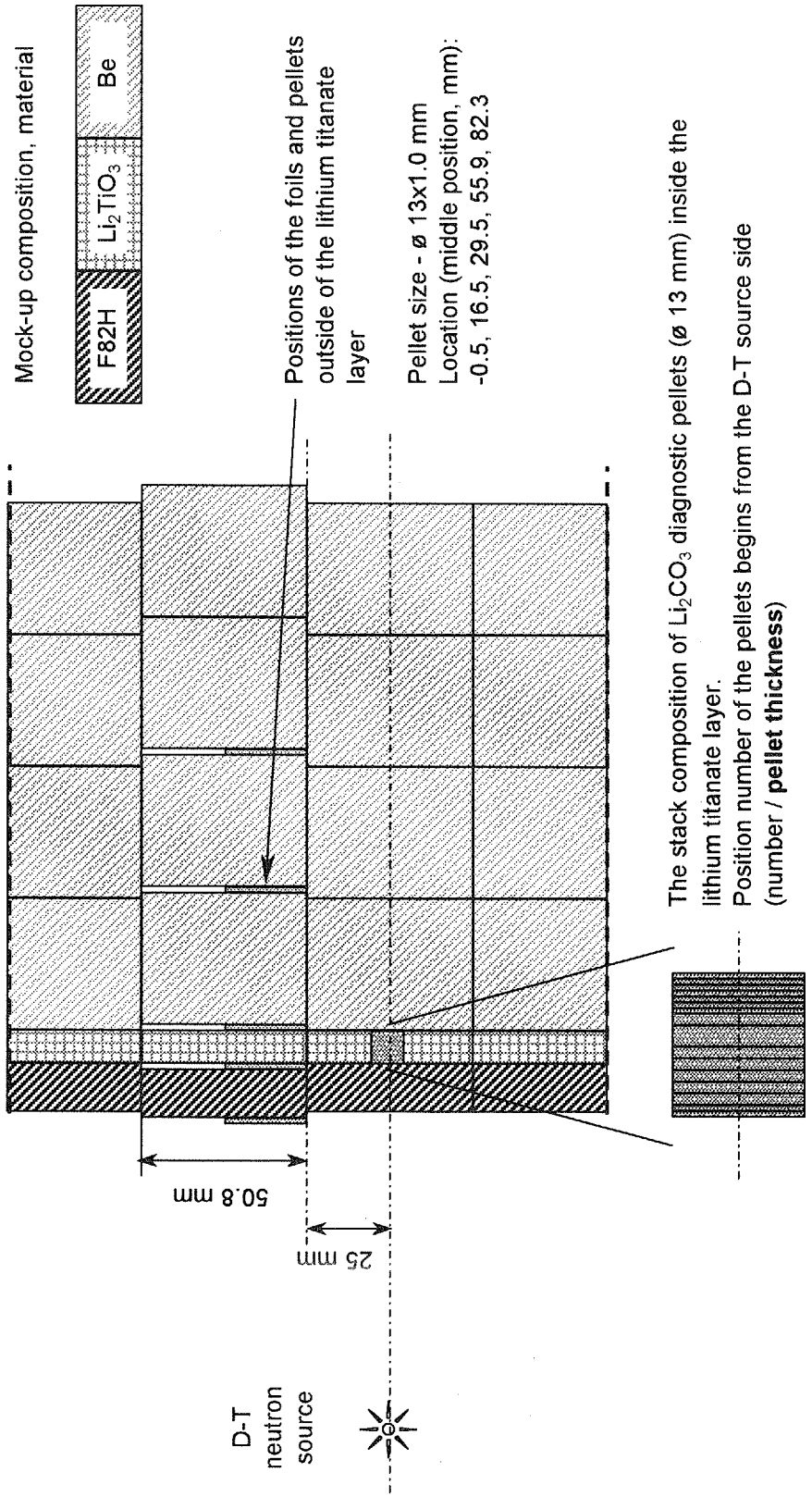

Figure 5. Arrangement of pellets and foils for reaction rates measurement inside the blanket mock-up

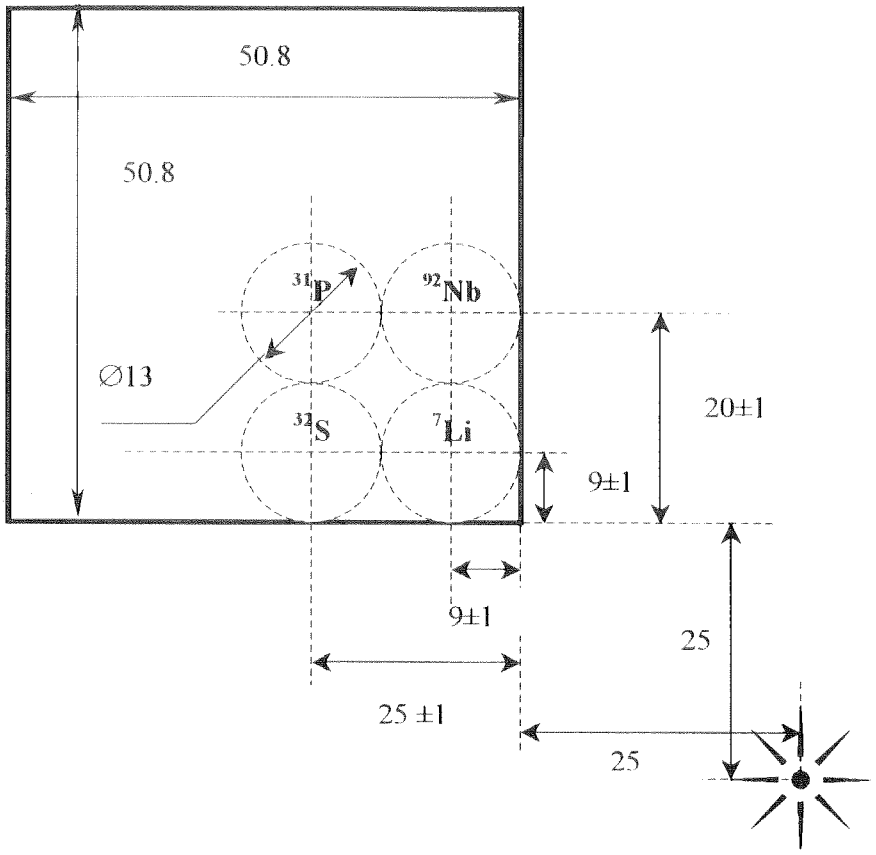

Figure 6. Pellet positions on the plate (or block) surface relative to the central axis of the mock-up.

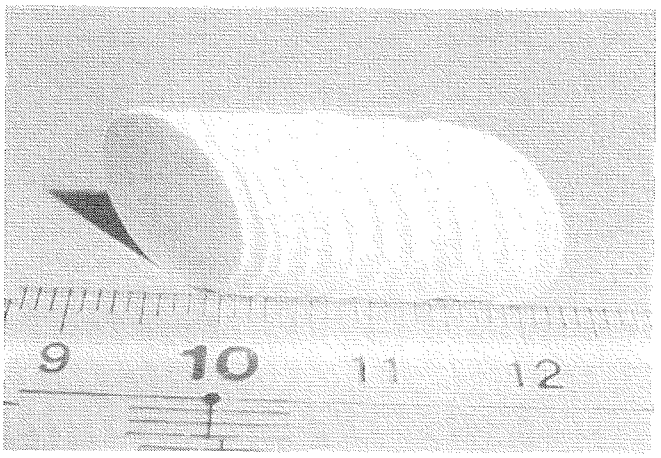

Figure 7. A stack of diagnostic Li_2CO_3 pellets for measurements of the tritium production rate inside the lithium titanate layer (pellets are specially reversed to highlight their various thicknesses).

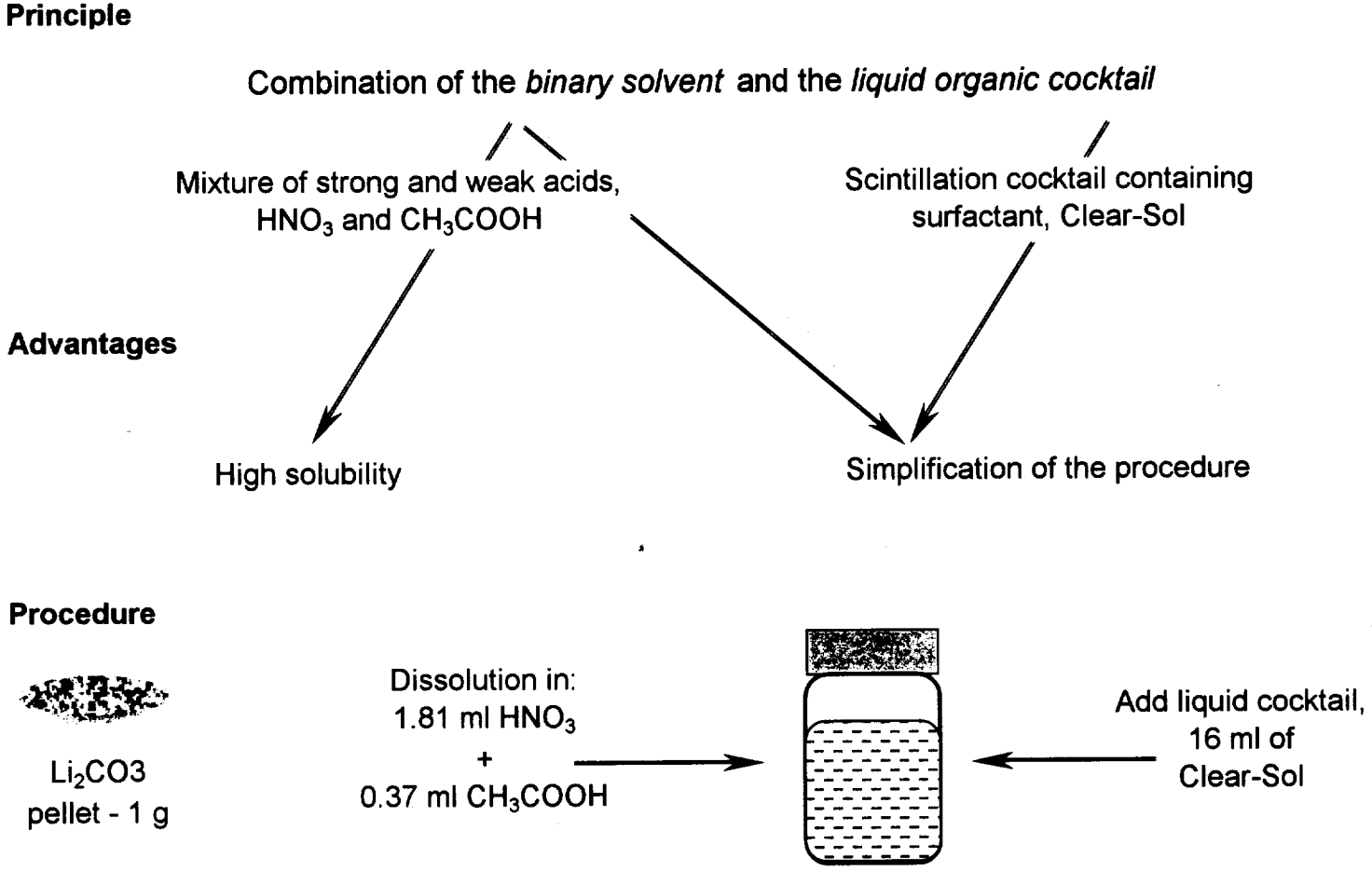

Figure 8. Direct technique for measurement of tritium activity in the diagnostic pellet.

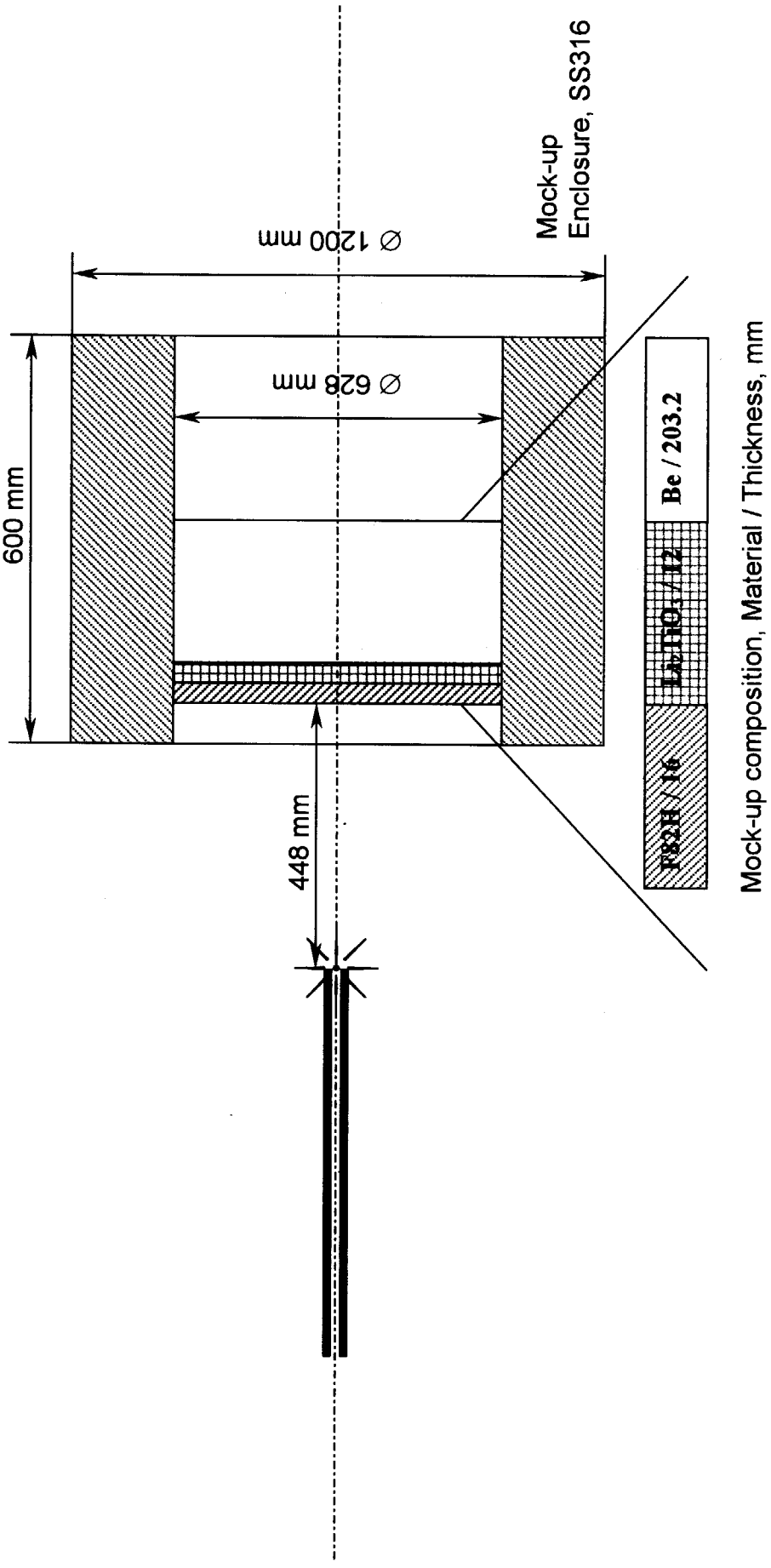

Figure 9. Experimental configuration of the experiment on the blanket mock-up irradiated by neutrons from the D-T source.

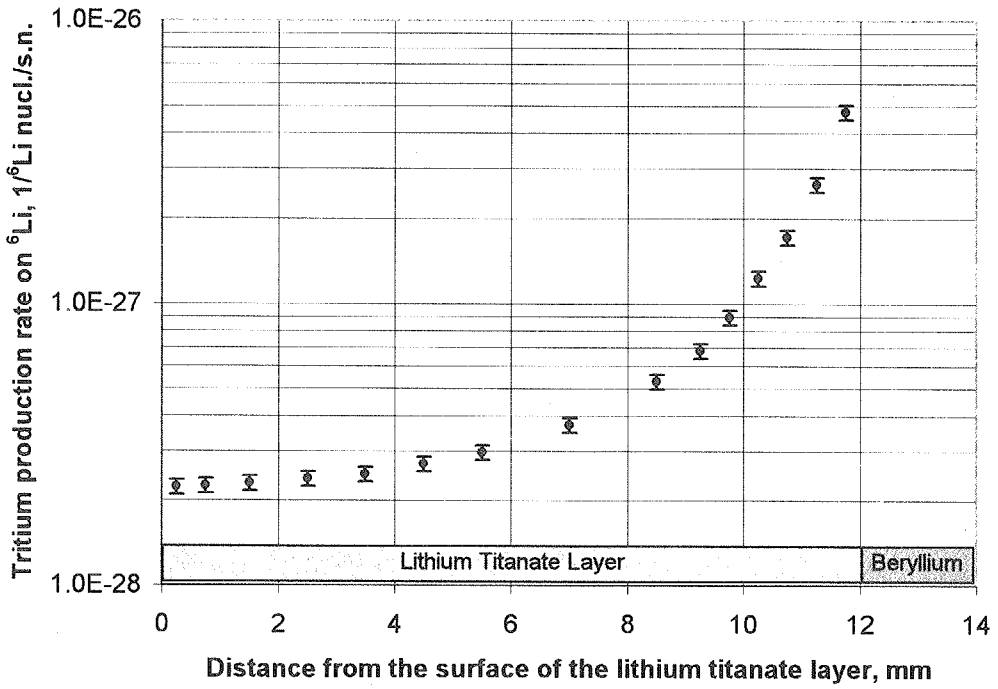

Figure 10. Tritium production rate distribution via the $^{6}Li(n,\alpha)^{3}H$ reaction inside the lithium titanate layer of the mock-up irradiated by neutrons from the D-T source.

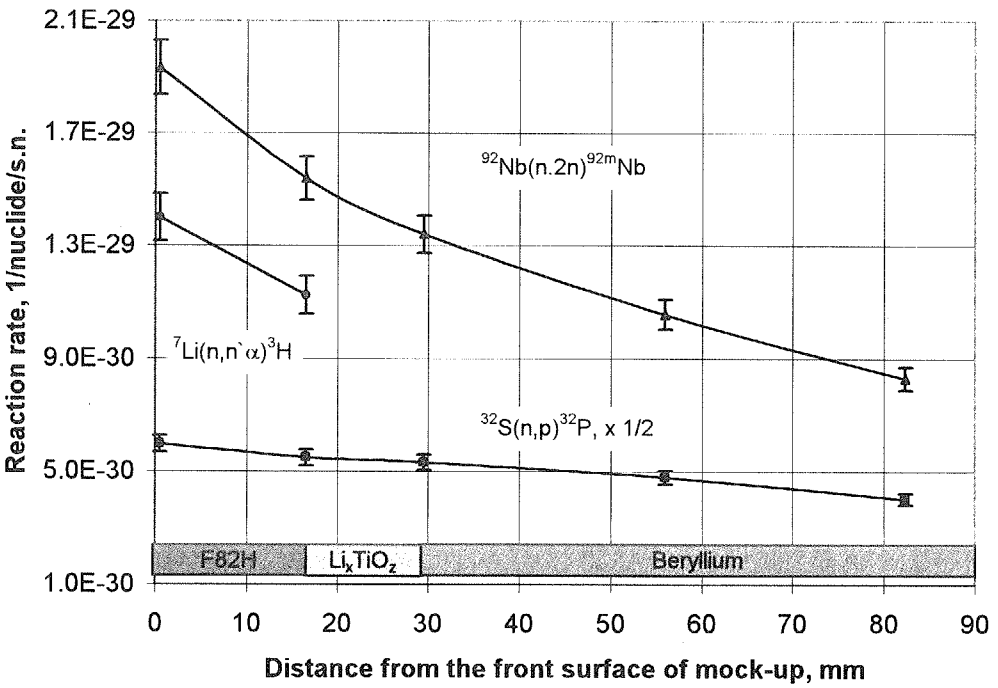

Figure 11. Distribution of reaction rates sensitive to fast neutrons in the blanket mock-up irradiated by neutrons from the D-T source.

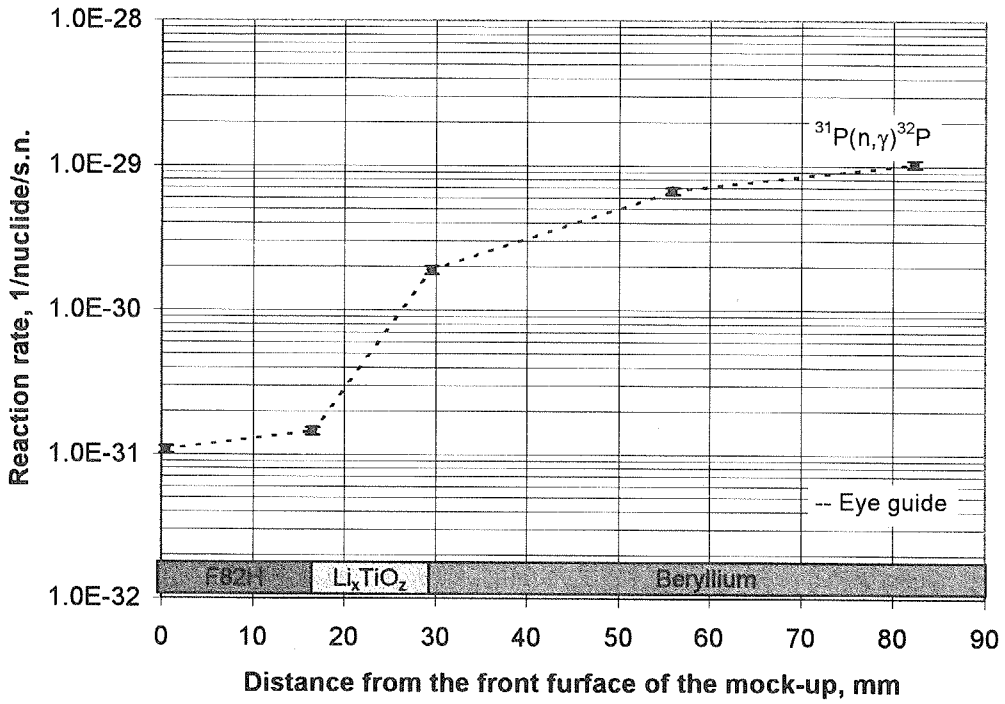

Figure 12. Distribution of the reaction rate sensitive to slow neutrons in the blanket mock-up irradiated by neutrons from the D-T source.

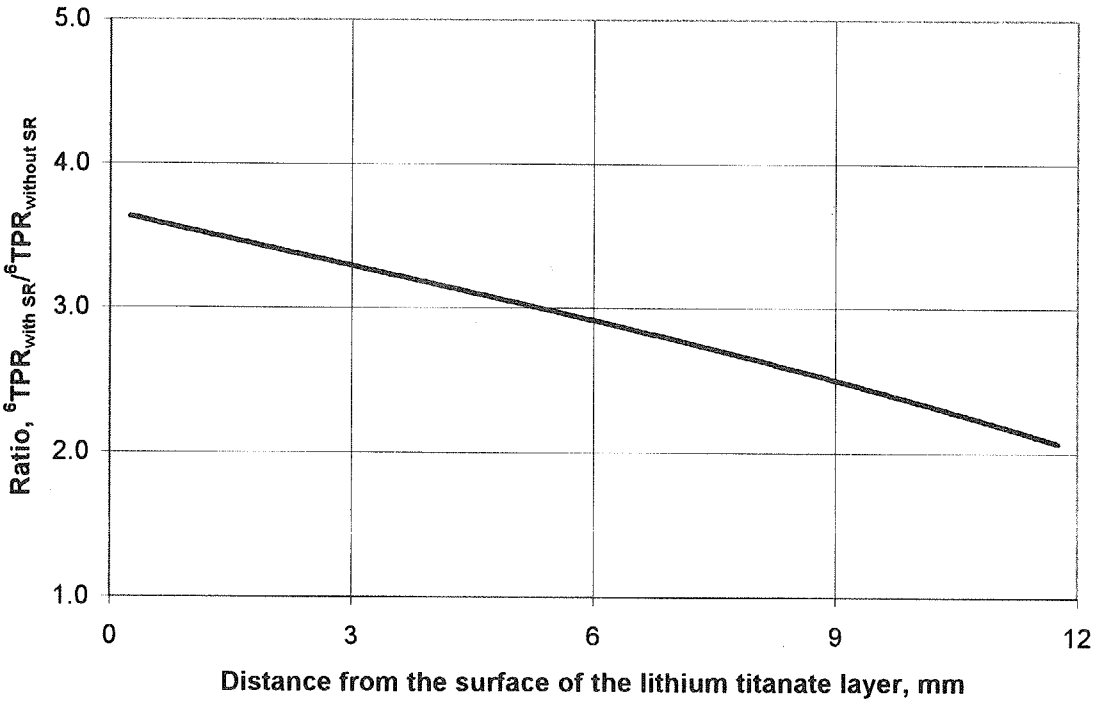

Figure 13. The source reflector effect on TPR in the lithium titanate layer

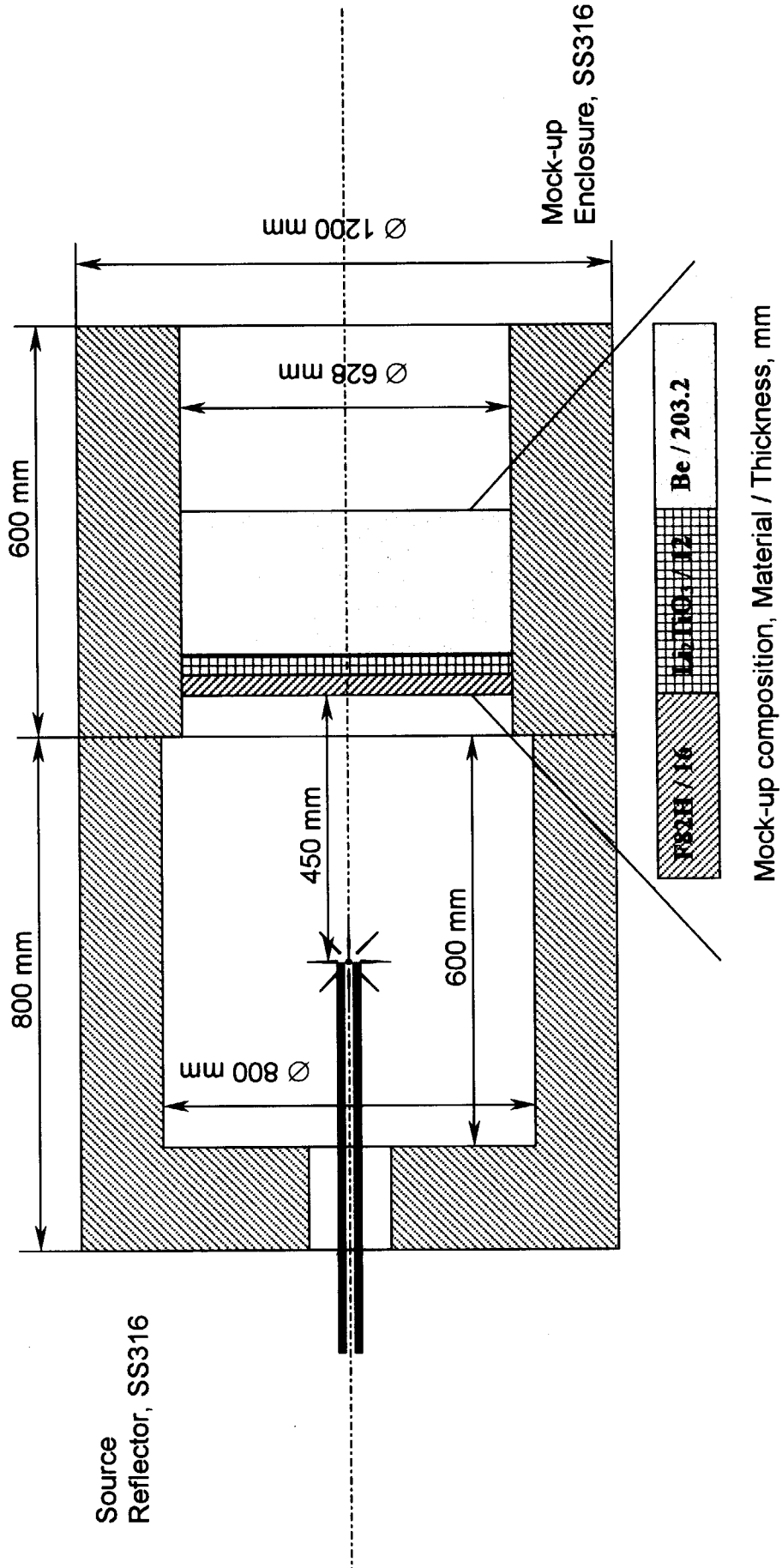

Figure 14. Experimental configuration of the experiment on the blanket mock-up irradiated by neutrons from the D-T source with a reflector.

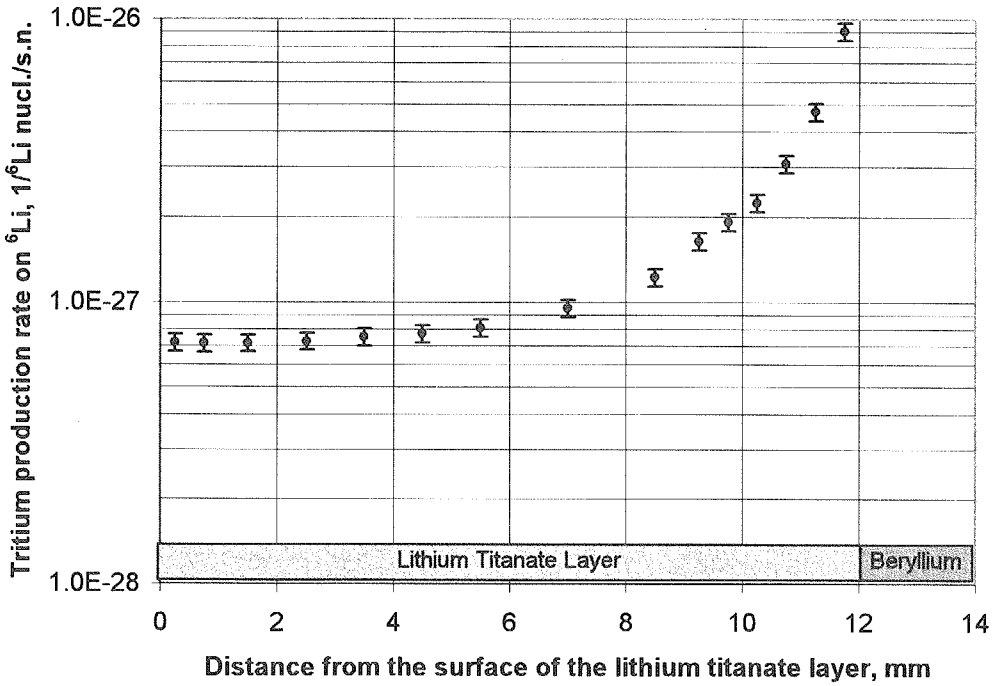

Figure 15. Tritium production rate distribution via the $^{6}Li(n,\alpha)^{3}H$ reaction inside the lithium titanate layer of the blanket mock-up irradiated by neutrons from the D-T source with a reflector.

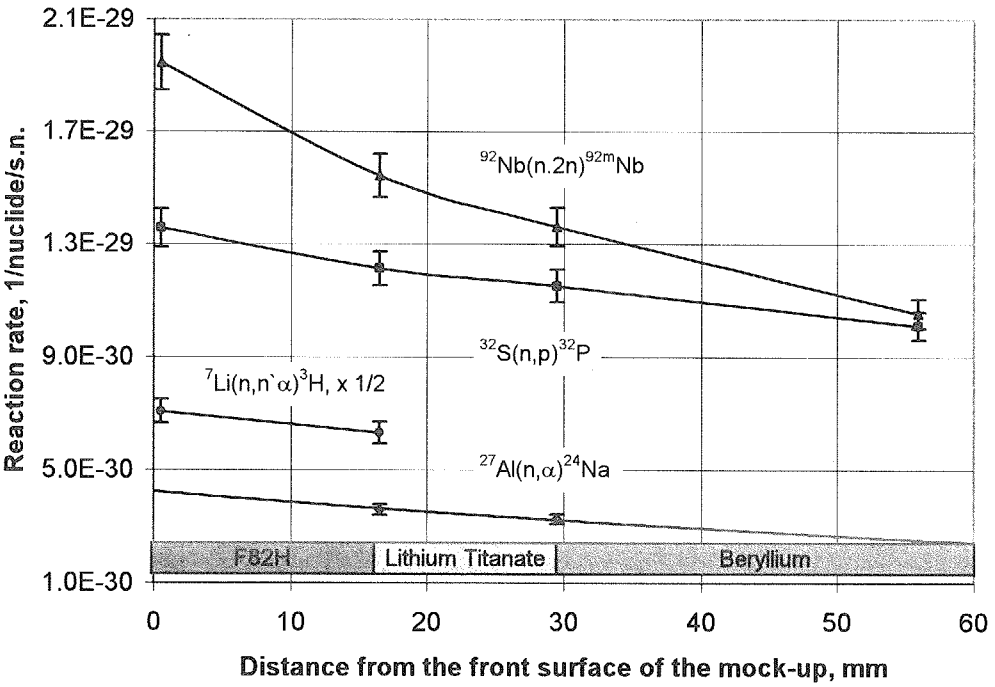

Figure 16. Distribution of reaction rates sensitive to fast neutrons in the blanket mock-up irradiated by neutrons from the D-T source with a reflector.

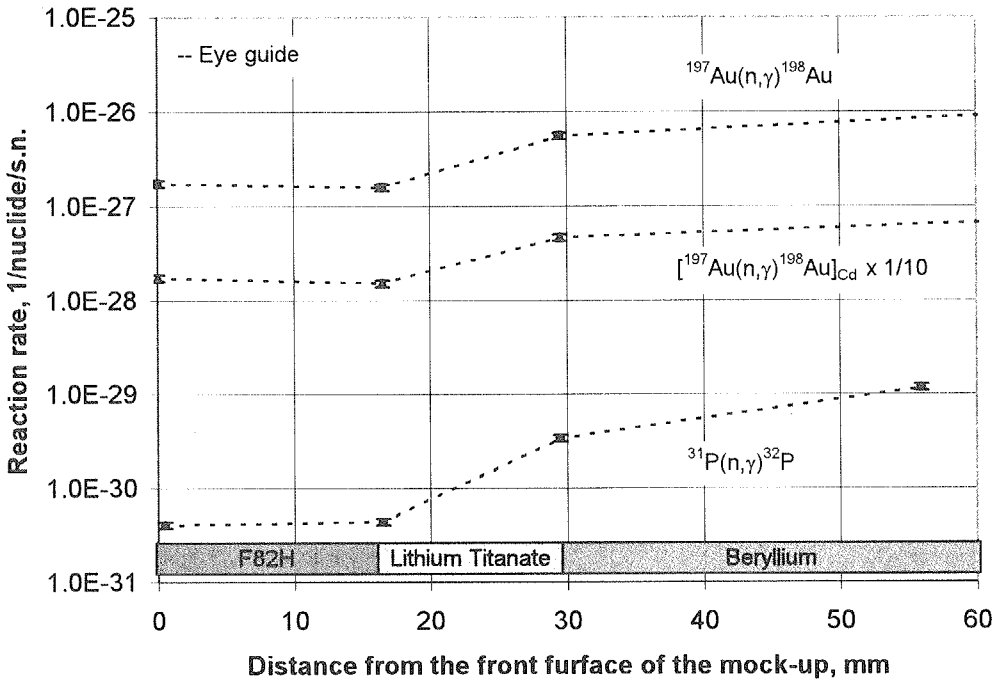

Figure 17. Distribution of the reaction rates sensitive to slow neutrons in the blanket mock-up irradiated by neutrons from the D-T source with a reflector.

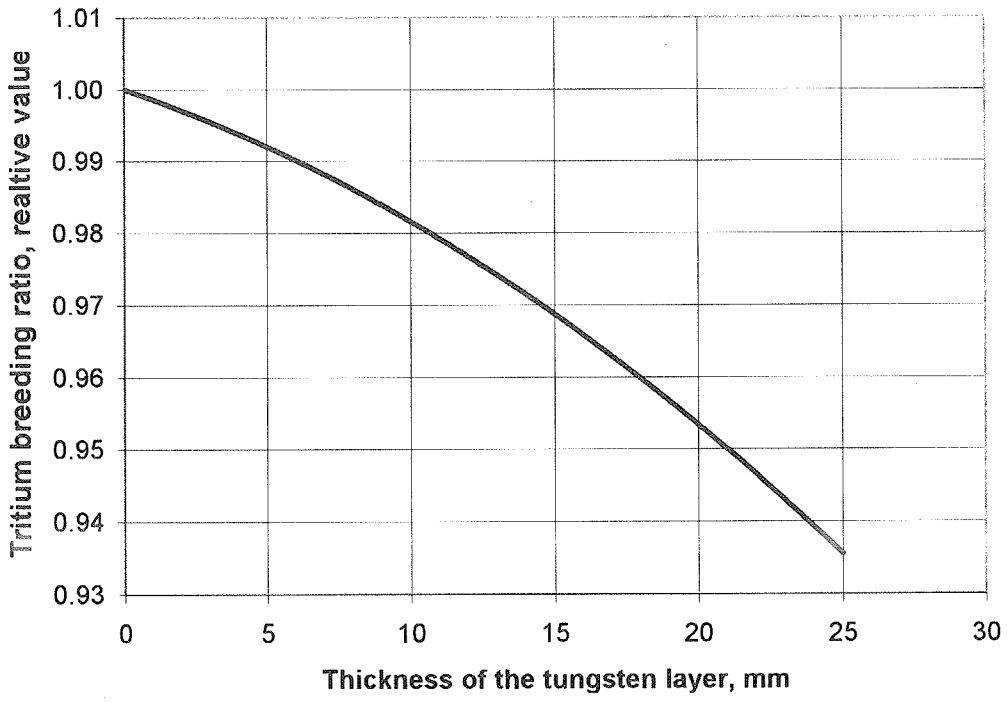

Figure 18. The tungsten armor effect on tritium production for various tungsten layer thicknesses.

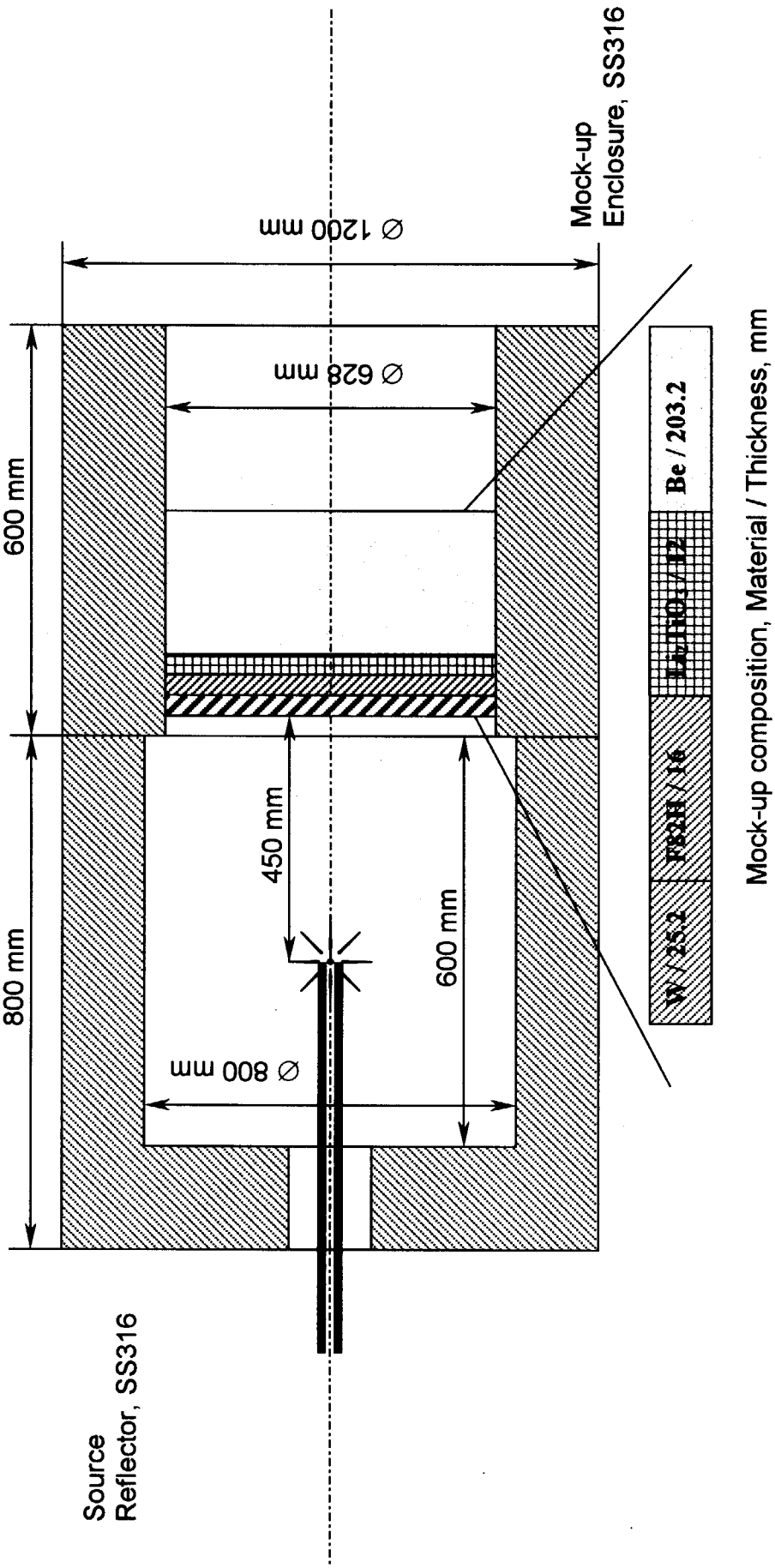

Figure 19. Experimental configuration of the experiment on the blanket mock-up with a tungsten layer irradiated by neutrons from the D-T source with a reflector.

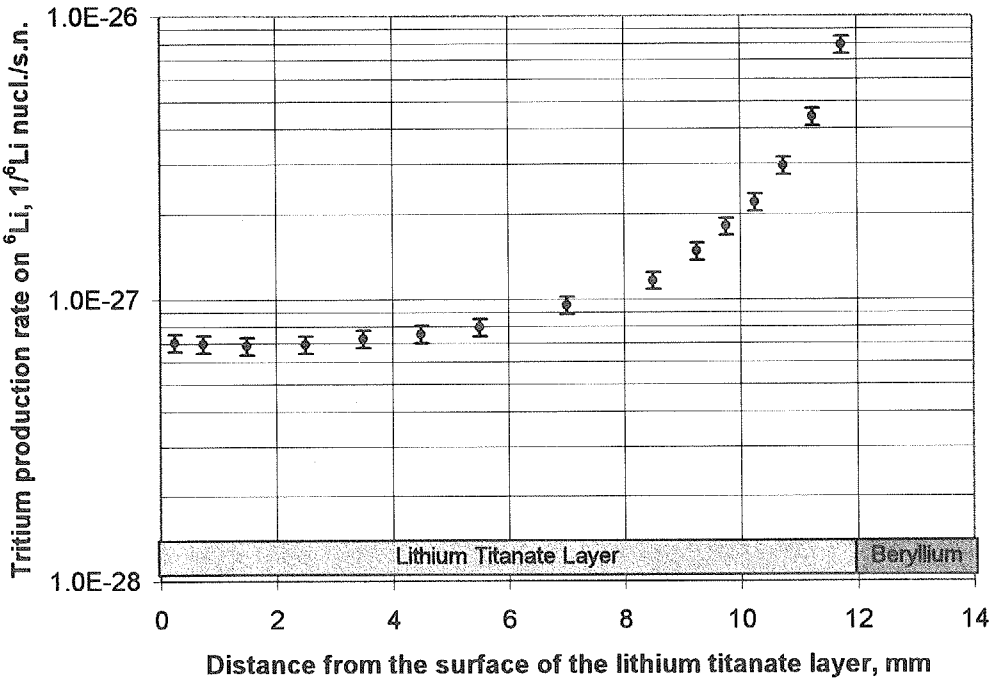

Figure 20. Tritium production rate distribution via the ^{6}Li(n,α)^{3}H reaction inside the lithium titanate layer of the blanket mock-up with a tungsten layer irradiated by neutrons from the D-T source with a reflector.

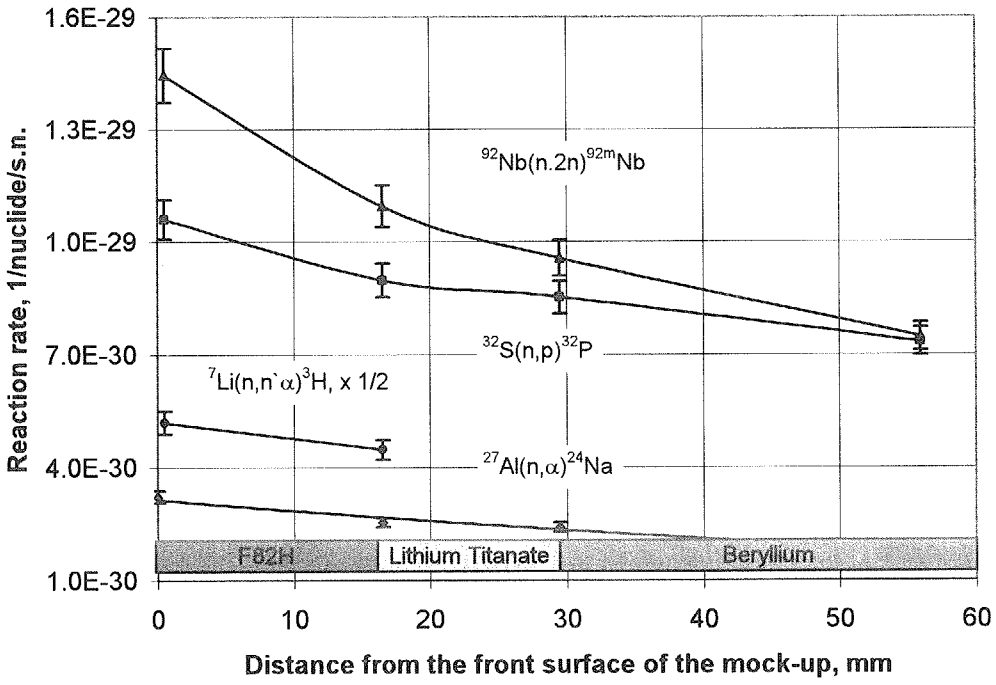

Figure 21. Distribution of the reaction rates sensitive to fast neutrons in the blanket mock-up with a tungsten layer irradiated by neutrons from the D-T source with a reflector.

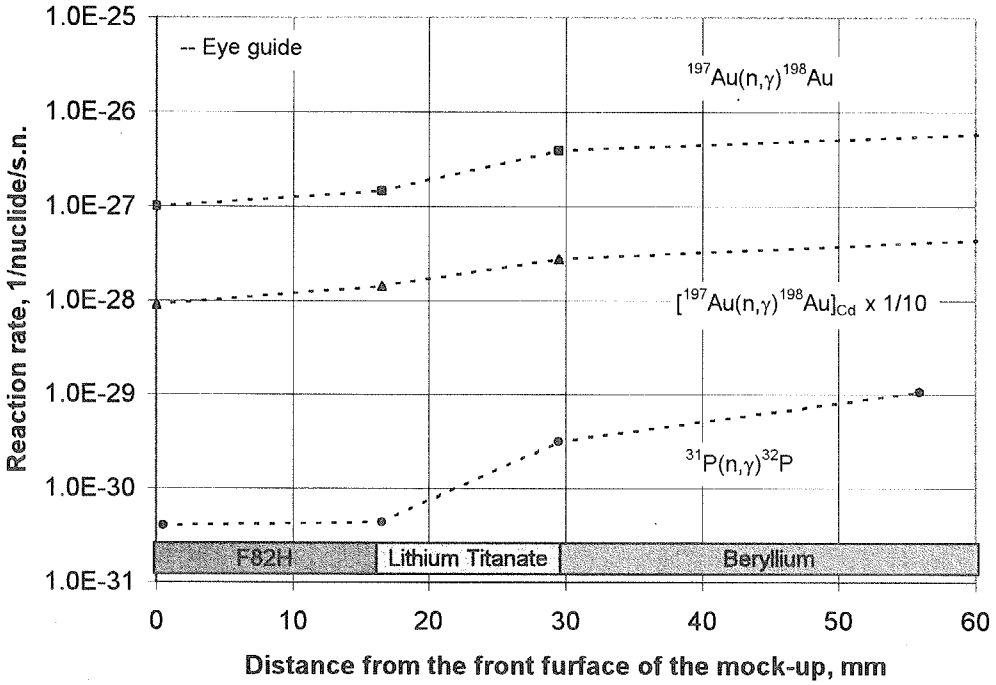

Figure 22. Distribution of the reaction rate sensitive to slow neutrons in the blanket mock-up with a tungsten layer irradiated by neutrons from the D-T source with a reflector.

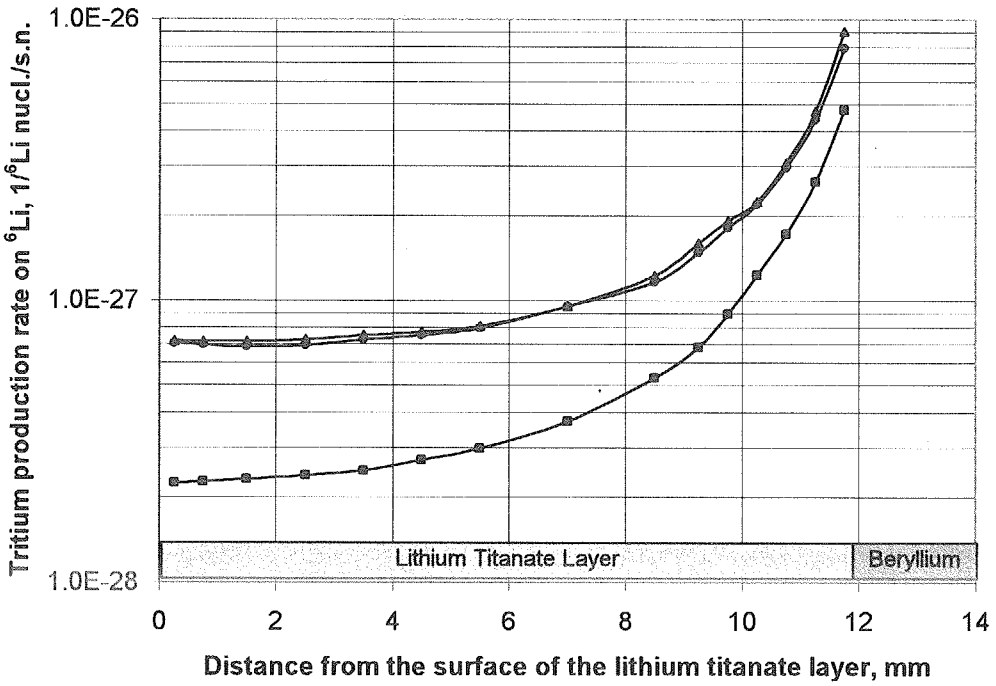

Figure 23. Comparison of the TPR-6 in three integral experiments on the blanket mock-up: without a tungsten layer and a source reflector (squares); with a source reflector and a tungsten layer (circles); with a source reflector and without a tungsten layer (triangle).

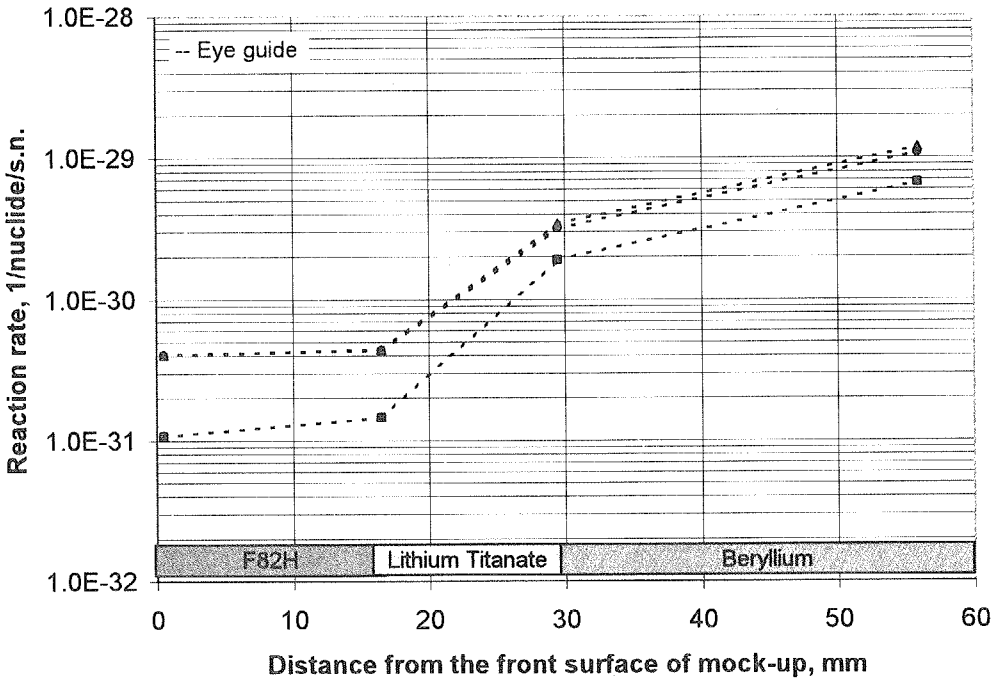

Figure 24. Comparison of the $^{31}P(n,\gamma)^{32}P$ reaction rate in three integral experiments on the blanket mock-up: without a tungsten layer and a source reflector (squares); with a source reflector and a tungsten layer (circles); with a source reflector and without a tungsten layer (triangle).

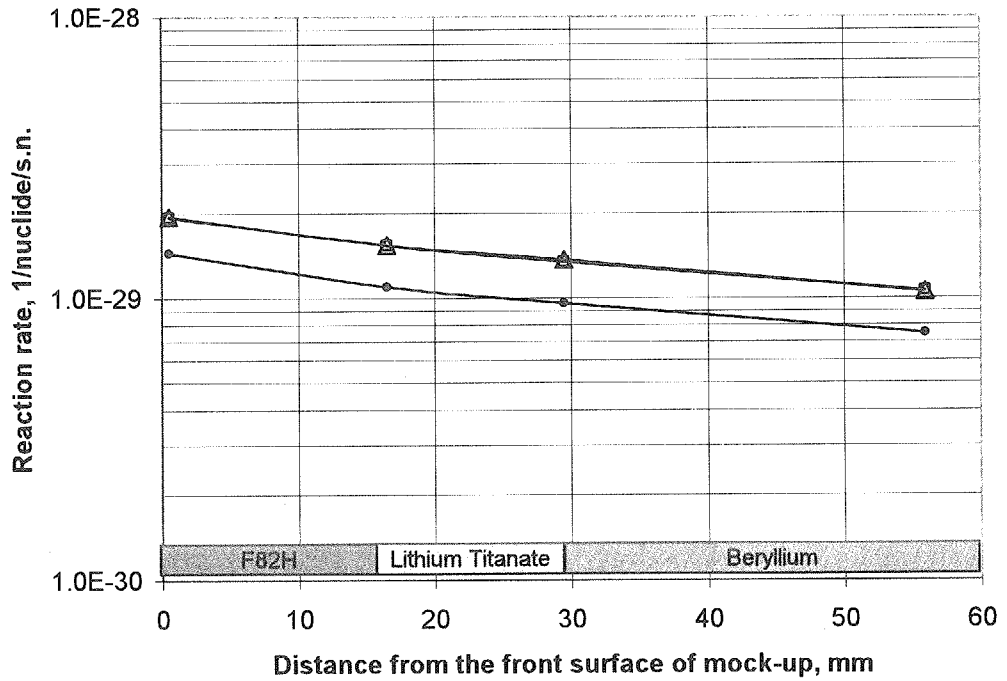

Figure 25. Comparison of the $^{93}Nb(n,2n)^{92m}Nb$ reaction rate in three integral experiments on the blanket mock-up: without a tungsten layer and a source reflector (squares); with a source reflector and a tungsten layer (circles); with a source reflector and without a tungsten layer (triangle).

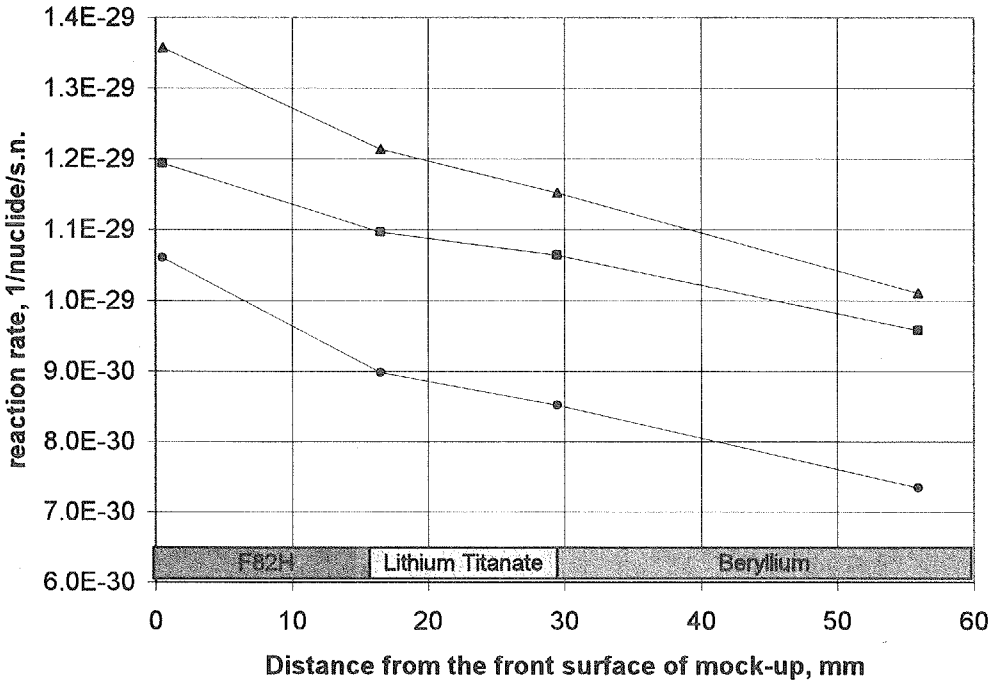

Figure 26. Comparison of the $^{32}S(n,p)^{32}P$ reaction rate in three integral experiments on the blanket mock-up: without a tungsten layer and a source reflector (squares); with a source reflector and a tungsten layer (circles); with a source reflector and without a tungsten layer (triangle).

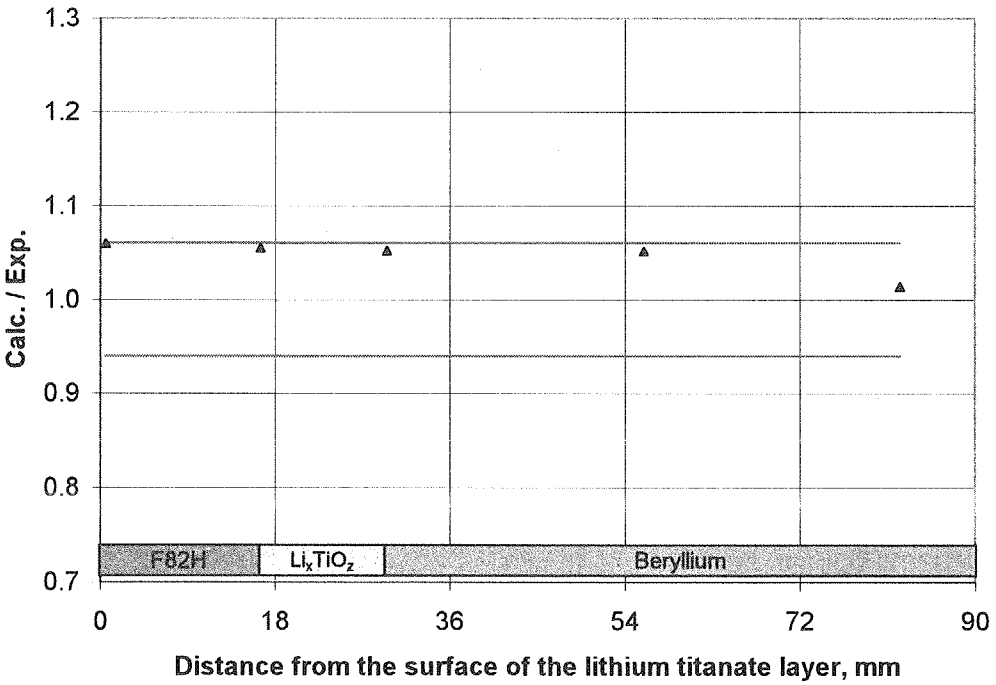

Figure 27. The calculated to experimental rate ratio for $^{93}Nb(n,2n)^{92m}Nb$ reaction in the blanket mock-up irradiated by neutrons from D-T source.

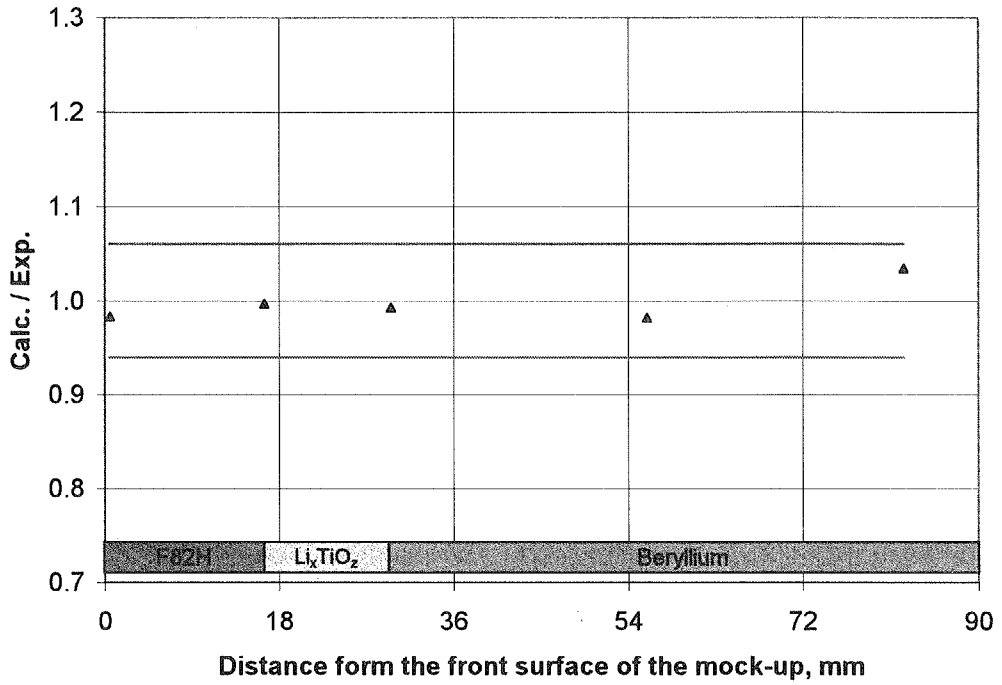

Figure 28. The calculated to experimental rate ratio for $^{32}S(n,p)^{32}P$ reaction in the blanket mock-up irradiated by neutrons from D-T source.

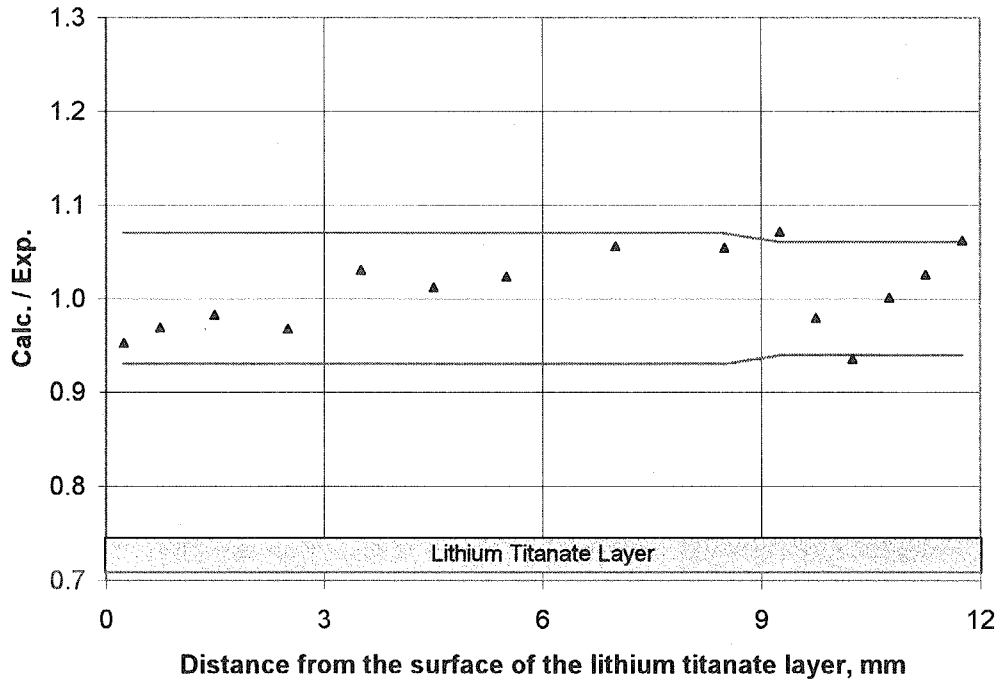

Figure 29. The calculated to experimental TPR-6 value ratio inside the lithium titanate layer of the blanket mock-up irradiated by neutrons from D-T source.

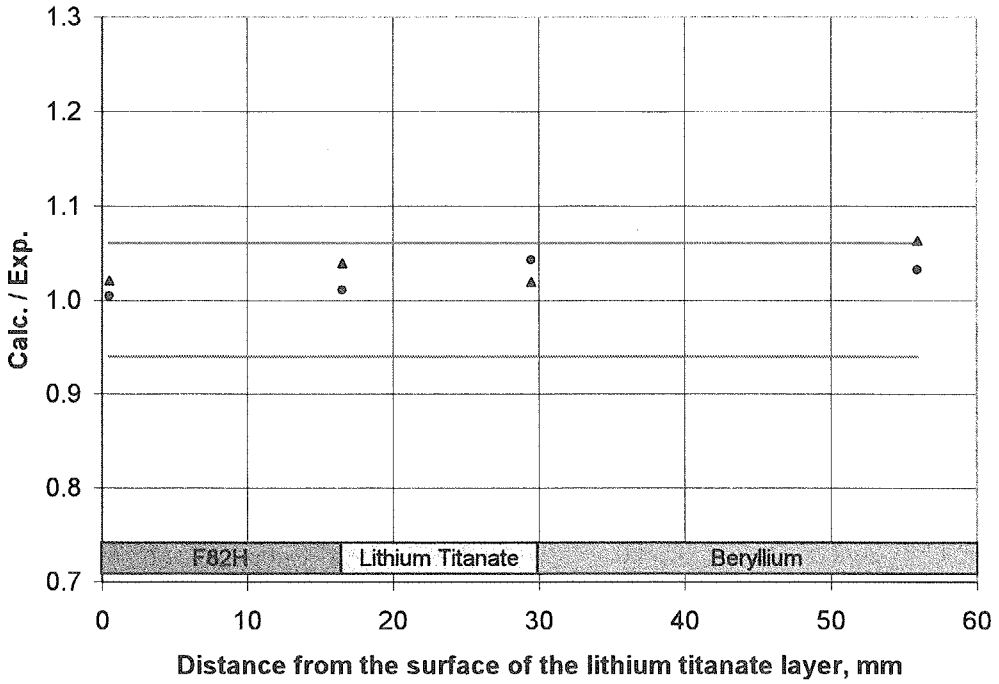

Figure 30. The calculated to experimental rate ratio for $^{93}Nb(n,2n)^{92m}Nb$ reaction in the blanket mock-up with (circles) and without (triangle) a tungsten layer irradiated by neutrons from the D-T source with a reflector.

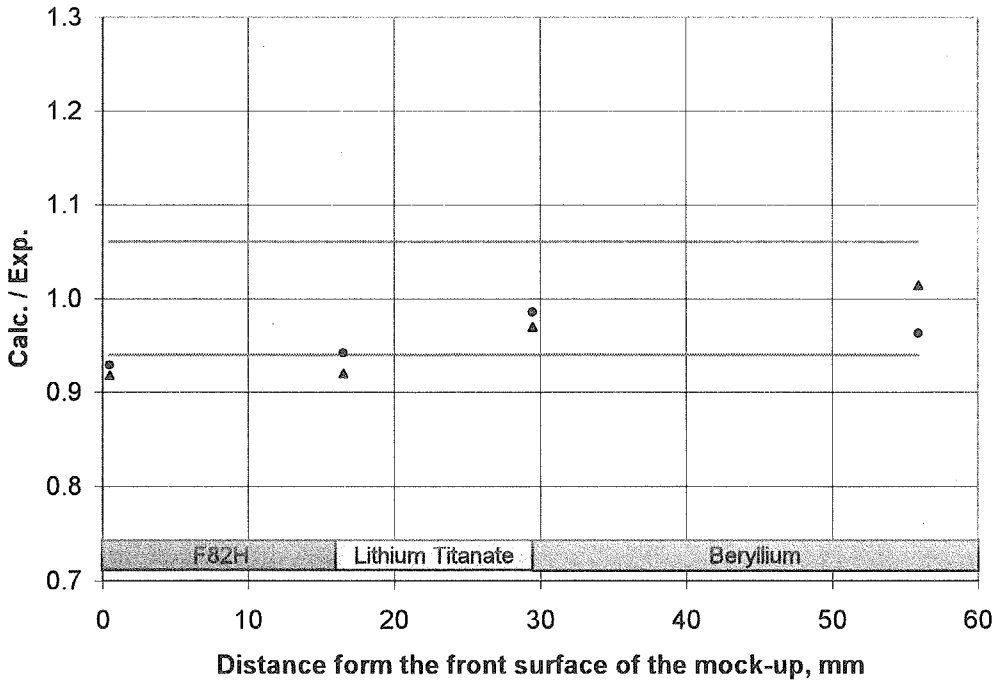

Figure 31. The calculated to experimental rate ratio for $^{32}S(n,p)^{32}P$ reaction in the blanket mock-up with (circles) and without (triangle) a tungsten layer irradiated by neutrons from the D-T source with a reflector.

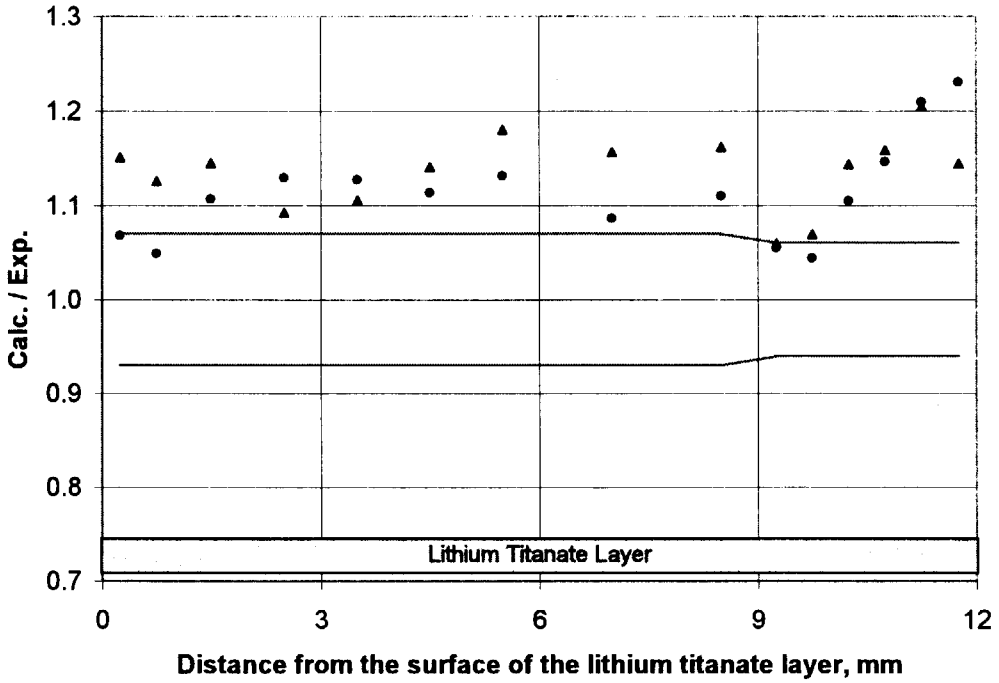

Figure 32. The calculated to experimental tritium production rate ratio on lithium-6 inside the lithium titanate layer of the blanket mock-up with (circles) and without (triangle) a tungsten layer irradiated by neutrons from the D-T source with a reflector.

This is a blank page.

国際単位系 (SI) と換算表

表 1　SI基本単位および補助単位

量	名称	記号
長さ	メートル	m
質量	キログラム	kg
時間	秒	s
電流	アンペア	A
熱力学温度	ケルビン	K
物質量	モル	mol
光度	カンデラ	cd
平面角	ラジアン	rad
立体角	ステラジアン	sr

表 2　SIと併用される単位

名称	記号
分，時，日	min，h，d
度，分，秒	°，′，″
リットル	l，L
トン	t
電子ボルト	eV
原子質量単位	u

1 eV = 1.60218 × 10^{-19} J

1 u = 1.66054 × 10^{-27} kg

表 5　SI接頭語

倍数	接頭語	記号
10^{18}	エクサ	E
10^{15}	ペタ	P
10^{12}	テラ	T
10^{9}	ギガ	G
10^{6}	メガ	M
10^{3}	キロ	k
10^{2}	ヘクト	h
10^{1}	デカ	da
10^{-1}	デシ	d
10^{-2}	センチ	c
10^{-3}	ミリ	m
10^{-6}	マイクロ	μ
10^{-9}	ナノ	n
10^{-12}	ピコ	p
10^{-15}	フェムト	f
10^{-18}	アト	a

表 3　固有の名称をもつSI組立単位

量	名称	記号	他のSI単位による表現
周波数	ヘルツ	Hz	s^{-1}
力	ニュートン	N	m·kg/s^2
圧力，応力	パスカル	Pa	N/m^2
エネルギー，仕事，熱量	ジュール	J	N·m
工率，放射束	ワット	W	J/s
電気量，電荷	クーロン	C	A·s
電位，電圧，起電力	ボルト	V	W/A
静電容量	ファラド	F	C/V
電気抵抗	オーム	Ω	V/A
コンダクタンス	ジーメンス	S	A/V
磁束	ウェーバ	Wb	V·s
磁束密度	テスラ	T	Wb/m^2
インダクタンス	ヘンリー	H	Wb/A
セルシウス温度	セルシウス度	℃	
光束	ルーメン	lm	cd·sr
照度	ルクス	lx	lm/m^2
放射能	ベクレル	Bq	s^{-1}
吸収線量	グレイ	Gy	J/kg
線量当量	シーベルト	Sv	J/kg

表 4　SIと共に暫定的に維持される単位

名称	記号
オングストローム	Å
バーン	b
バール	bar
ガル	Gal
キュリー	Ci
レントゲン	R
ラド	rad
レム	rem

1 Å = 0.1 nm = 10^{-10} m

1 b = 100 fm^2 = 10^{-28} m^2

1 bar = 0.1 MPa = 10^5 Pa

1 Gal = 1 cm/s^2 = 10^{-2} m/s^2

1 Ci = 3.7 × 10^{10} Bq

1 R = 2.58 × 10^{-4} C/kg

1 rad = 1 cGy = 10^{-2} Gy

1 rem = 1 cSv = 10^{-2} Sv

（注）

1. 表1－5は「国際単位系」第5版，国際度量衡局 1985年刊行による。ただし，1 eVおよび1 uの値はCODATAの1986年推奨値によった。
2. 表4には海里，ノット，アール，ヘクタールも含まれているが日常の単位なのでここでは省略した。
3. barは，JISでは流体の圧力を表わす場合に限り表2のカテゴリーに分類されている。
4. EC閣僚理事会指令ではbar，barnおよび「血圧の単位」mmHgを表2のカテゴリーに入れている。

換算表

	N(=10^5 dyn)	kgf	lbf
力	1	0.101972	0.224809
	9.80665	1	2.20462
	4.44822	0.453592	1

粘度　1 Pa·s(N·s/m^2) = 10 P(ポアズ)(g/(cm·s))

動粘度　1 m^2/s = 10^4 St(ストークス)(cm^2/s)

圧力	MPa(=10 bar)	kgf/cm^2	atm	mmHg(Torr)	lbf/in^2(psi)
	1	10.1972	9.86923	7.50062 × 10^3	145.038
	0.0980665	1	0.967841	735.559	14.2233
	0.101325	1.03323	1	760	14.6959
	1.33322 × 10^{-4}	1.35951 × 10^{-3}	1.31579 × 10^{-3}	1	1.93368 × 10^{-2}
	6.89476 × 10^{-3}	7.03070 × 10^{-2}	6.80460 × 10^{-2}	51.7149	1

エネルギー・仕事・熱量	J(=10^7 erg)	kgf·m	kW·h	cal(計量法)	Btu	ft·lbf	eV
	1	0.101972	2.77778 × 10^{-7}	0.238889	9.47813 × 10^{-4}	0.737562	6.24150 × 10^{18}
	9.80665	1	2.72407 × 10^{-6}	2.34270	9.29487 × 10^{-3}	7.23301	6.12082 × 10^{19}
	3.6 × 10^6	3.67098 × 10^5	1	8.59999 × 10^5	3412.13	2.65522 × 10^6	2.24694 × 10^{25}
	4.18605	0.426858	1.16279 × 10^{-6}	1	3.96759 × 10^{-3}	3.08747	2.61272 × 10^{19}
	1055.06	107.586	2.93072 × 10^{-4}	252.042	1	778.172	6.58515 × 10^{21}
	1.35582	0.138255	3.76616 × 10^{-7}	0.323890	1.28506 × 10^{-3}	1	8.46233 × 10^{18}
	1.60218 × 10^{-19}	1.63377 × 10^{-20}	4.45050 × 10^{-26}	3.82743 × 10^{-20}	1.51857 × 10^{-22}	1.18171 × 10^{-19}	1

1 cal = 4.18605 J(計量法)

= 4.184 J　(熱化学)

= 4.1855 J　(15 °C)

= 4.1868 J(国際蒸気表)

仕事率　1 PS(仏馬力)

= 75 kgf·m/s

= 735.499 W

放射能	Bq	Ci
	1	2.70270 × 10^{-11}
	3.7 × 10^{10}	1

吸収線量	Gy	rad
	1	100
	0.01	1

照射線量	C/kg	R
	1	3876
	2.58 × 10^{-4}	1

線量当量	Sv	rem
	1	100
	0.01	1

（86年12月26日現在）

Integral Experiments for Verification of Tritium Production on the Beryllium/Lithium Titanate Blanket Mock-up with a One-breeder Layer

R50
古紙配合率100%
白色度70%の再生紙を使用しています